

Article

Softsign-Based Nonlinear Control of Steam Condenser via Gbest-Guided Atom and Pattern Search Approach

Davut Izci ^{1,*} , Serdar Ekinçi ², Emre Çelik ³ , Behçet Kocaman ⁴ and Erdal Akin ^{2,5,6,7,*}

- ¹ Department of Electrical and Electronic Engineering, Bursa Uludağ University, Bursa 16059, Turkey
² Department of Computer Engineering, Bitlis Eren University, Bitlis 13100, Turkey; sekinci@beu.edu.tr
³ Department of Electrical and Electronics Engineering, Düzce University, Düzce 81620, Turkey; emrecelik@duzce.edu.tr
⁴ Department of Electrical and Electronics Engineering, Bitlis Eren University, Bitlis 13100, Turkey; bkocaman@beu.edu.tr
⁵ Department of Computer Science and Media Technology, Malmö University, 205 06 Malmö, Sweden
⁶ Sustainable Digitalisation Research Centre, Malmö University, 205 06 Malmö, Sweden
⁷ Biofilms Research Center for Biointerfaces (BRCB), Malmö University, 205 06 Malmö, Sweden
* Correspondence: davutizci@uludag.edu.tr (D.I.); erdal.akin@mau.se (E.A.)

Abstract

This paper introduces a novel cascaded softsign function-based PID (CSoft-PID) controller designed for precise pressure regulation in highly nonlinear shell-and-tube steam condenser systems. For the first time in the literature, the classical PID control structure is enhanced through a cascaded nonlinear transformation using the softsign function, which dynamically adjusts the controller input according to the magnitude of the error. This architecture allows for high sensitivity near the setpoint while gracefully limiting excessive control efforts during larger deviations, thereby improving stability and transient performance. To optimally tune the six parameters of the proposed controller, a new hybrid optimization algorithm, termed hGASO-PS, is proposed. This method synergistically integrates an adaptive gbest-guided atom search optimization (ASO) strategy with the precision of the pattern search (PS) technique, ensuring both effective global exploration and fine-tuned local exploitation. The controller parameters are optimized by minimizing the integral of time-weighted absolute error (ITAE), subject to a step change in the condenser pressure setpoint. Extensive simulations and statistical evaluations demonstrate the superiority of the proposed approach. The hGASO-PS-based CSoft-PID controller achieved the lowest ITAE value of 2.1608, with an average of 2.2746 across 30 runs. It also demonstrated the fastest settling time (12.51 s) and the lowest overshoot (1.98%) among all tested controllers. Comparisons with recent PI, FOPID, and cascaded PI-PDN controllers confirm the consistent outperformance of the proposed method in both transient response and control precision, making it a promising candidate for industrial condenser applications.

Keywords: nonlinear optimization problem; pressure regulation of steam condenser; softsign function-based PID controller; atom search optimization; pattern search



Academic Editor: José Matas

Received: 25 February 2026

Revised: 18 March 2026

Accepted: 19 March 2026

Published: 22 March 2026

Copyright: © 2026 by the authors.

Licensee MDPI, Basel, Switzerland.

This article is an open access article distributed under the terms and conditions of the [Creative Commons Attribution \(CC BY\)](https://creativecommons.org/licenses/by/4.0/) license.

1. Introduction

Shell-and-tube steam condensers are vital components in thermal, nuclear, and marine power plants, playing a key role in converting exhaust steam from turbines back into water, thereby completing the energy cycle [1]. Given their central role, maintaining stable pressure within these systems is essential for ensuring thermodynamic efficiency,

operational safety, and system reliability. However, the intrinsic dynamics of these condensers are far from linear. The interaction of steam, non-condensable gases, condensate, and cooling water introduces complex, nonlinear behaviors that challenge conventional control strategies.

Over the years, researchers have explored various control strategies to enhance the performance and stability of heat exchanger systems. For example, Nithya et al. [2] investigated the application of predictive control strategies for a shell-and-tube heat exchanger. Their study highlighted the effectiveness of model predictive control (MPC) in handling multivariable systems with constraints, offering improved setpoint tracking and disturbance rejection compared to traditional PID controllers. Pandey et al. [3] designed a fuzzy logic controller for a cross-flow shell-and-tube heat exchanger. The fuzzy controller demonstrated superior performance in managing the nonlinear behavior of the system, providing better temperature regulation and reduced overshoot compared to conventional control methods. Ahn et al. [4] proposed a proportional–integral–derivative (PID) control scheme incorporating feedforward control and anti-windup techniques for a shell-and-tube heat exchanger system. Their approach effectively mitigated the adverse effects of actuator saturation and improved the overall system response, ensuring stability and robustness under varying operating conditions. Wang and Li [5] applied particle swarm optimization (PSO) to tune PID controller parameters for a steam condenser system. The PSO-based PID controller achieved enhanced performance metrics, including reduced settling time and overshoot, demonstrating the potential of metaheuristic algorithms in control parameter optimization. Reddy and Balaji [6] utilized a genetic algorithm (GA) to optimize PID controller settings for temperature control in a shell-and-tube heat exchanger. The GA-PID controller outperformed traditional tuning methods, offering improved transient response and stability. Al-Dhaifallah [7] introduced a fuzzy fractional-order PID (FOPID) controller for heat exchanger systems. The integration of fuzzy logic with fractional calculus provided a more flexible control structure, capable of handling system uncertainties and nonlinearities effectively. Schiavo et al. [8] explored the application of PID acceleration (PIDA) control for heat exchangers. Their study demonstrated that PIDA controllers could offer improved dynamic performance, particularly in systems requiring rapid response and high precision. Jabari et al. [9] proposed a novel TDn(1+PIDn) controller optimized using a diligent crow search algorithm (DCSA) for pressure regulation in nonlinear shell-and-tube steam condensers. Their approach achieved significant improvements in control accuracy and response time, highlighting the efficacy of combining advanced control structures with bio-inspired optimization techniques.

Traditional controllers, such as the PID [10] family, have long been favored in industrial applications due to their simplicity and effectiveness. Yet, their linear nature often limits their adaptability in systems with time-varying nonlinearities. In the context of steam condensers, this may result in slower response times, excessive overshoot, or even instability, particularly under load disturbances or setpoint changes.

Over the decades, numerous enhancements have been introduced to improve PID performance in the face of nonlinear dynamics, time delays, and system uncertainties. These include robust control extensions, such as H_∞ control [11], sliding mode control [12], and FOPID controllers, that provide greater tuning flexibility [13,14]. Researchers have also proposed fuzzy-PID and optimal fuzzy-based PID controllers to handle complex nonlinearities and ensure smoother control actions under varying conditions [15,16].

The integration of intelligent optimization techniques with PID design has led to further performance improvements. For example, PSO [17], GA [6], and hybrid evolutionary approaches have been employed to automatically tune PID gains for various nonlinear processes, ranging from exoskeletons [17] and pressure systems [16] to power system

stabilizers [18]. More recent innovations include sigmoid-based [18,19], exponential [20], and reinforcement learning-enhanced structures [21], which aim to adaptively modulate control intensity based on system states or learned behavior. Multi-stage and cascaded PID variants have also gained popularity for improving disturbance rejection and transient response, particularly in voltage regulation [22,23], renewable-integrated systems [24,25], and converter dynamics [26,27].

Despite the breadth of these advancements, the majority of existing techniques still rely on either gain tuning of conventional PID structures or indirect shaping via approximation techniques. To address these challenges, the present study introduces a novel cascaded softsign function-based PID (CSoft-PID) controller, designed specifically for nonlinear condenser systems. This is the first time such a cascaded nonlinear transformation has been integrated into a PID framework using the softsign function [28]. By shaping the input signal through a smooth, saturating nonlinearity, the proposed controller enhances sensitivity near the setpoint while preventing aggressive control actions when large errors occur. This adaptive shaping mechanism ensures smoother transitions and improved damping without compromising responsiveness.

Equally important is the tuning of the controller's parameters, which must be meticulously calibrated to achieve the desired performance in a nonlinear environment. In response to this need, the study further proposes a new hybrid optimization algorithm, the hybrid adaptive gbest-guided atom search optimization and pattern search (hGASO-PS). This method blends the global search [29] capabilities of an improved atom search optimization algorithm [30] with the local refinement precision of pattern search [31]. The result is a well-balanced optimizer that overcomes the stagnation and slow convergence typically associated with standalone metaheuristics.

To verify the effectiveness of the proposed control scheme, extensive simulation experiments were conducted. The CSoft-PID controller, tuned via hGASO-PS, was benchmarked against several state-of-the-art PI, FOPID, and cascaded PI-PDN controllers from recent literature. The evaluations covered both statistical optimization metrics and closed-loop transient performance. Notably, the proposed approach achieved the lowest integral of time-weighted absolute error value (2.1608), the shortest settling time (12.51 s), and the smallest overshoot (1.98%), outperforming a broad range of recent control strategies.

The remainder of this paper is structured as follows: Section 2 introduces the dynamic modeling of the nonlinear steam condenser system. Section 3 discusses the fundamentals of the atom search optimization algorithm, while Section 4 presents the development of the proposed hGASO-PS. Section 5 details the novel CSoft-PID controller and its integration with the hybrid optimization framework. Section 6 reports the simulation results and comparative evaluations, and Section 7 concludes the paper with potential future directions.

2. Dynamic Modeling of Nonlinear Steam Condenser System

Shell-and-tube steam condensers are pivotal components within thermal, nuclear, and marine power plants, serving the critical role of condensing exhaust steam back into water for reuse within the power generation cycle [9]. The dynamic behavior of such condensers is inherently nonlinear due to the complex interactions between steam, non-condensable gases, cooling water, and the heat exchange surfaces. An accurate dynamic model is thus essential to ensure efficient control and to enhance system stability, energy efficiency, and operational safety [32].

The shell-and-tube condenser typically features a cylindrical or elliptical shell fitted with perforated tube plates and end closures that form water chambers [33]. Steam enters the upper section of the condenser through an inlet connected to the turbine exhaust, while cooling water flows through the tubes from the lower chambers. As steam contacts

the cooler surfaces of the water tubes, condensation occurs, releasing latent heat that is absorbed by the circulating cooling water. The resulting condensate is collected at the bottom in a hot well, while air and non-condensable gases are extracted through dedicated air outlets to maintain the necessary vacuum. A simplified schematic representation of the shell-and-tube steam condenser system is depicted in Figure 1 [33].

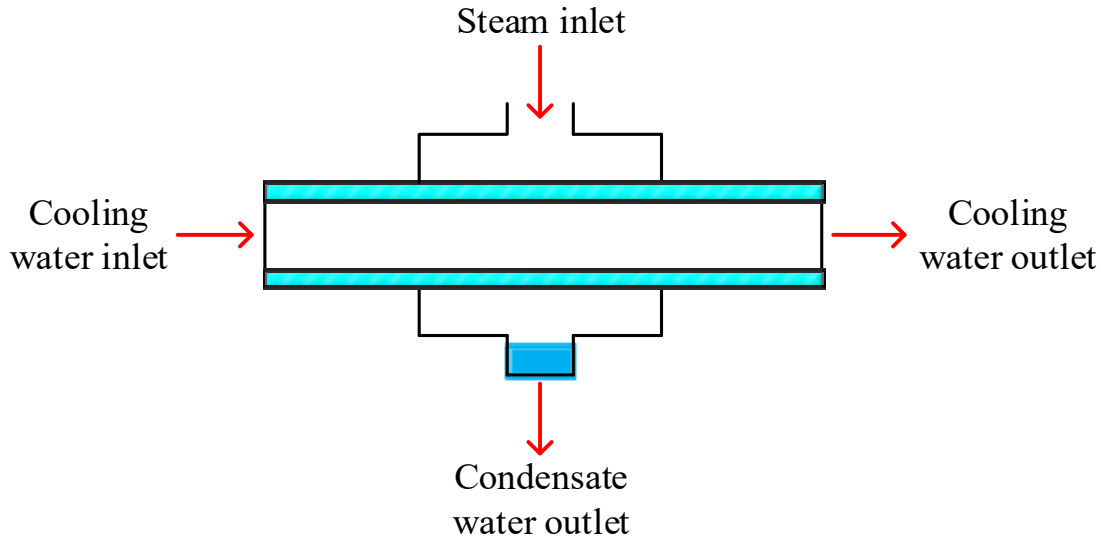


Figure 1. Simplified structure of the shell-and-tube steam condenser system.

2.1. *Mathematical Modeling of the Steam Zone*

The mass and energy balances within the steam zone are critical to understanding the condenser’s dynamic behavior. The mass conservation of the steam inside the shell can be expressed as:

$$\frac{dG_s}{dt} = G_{st} + G_{ost} + G_c - G_{ss} \tag{1}$$

where G_s denotes the steam mass inside the condenser, G_{st} is the steam flow rate from the turbine, G_{ost} is the additional steam input, G_c represents the condensate mass flow rate, and G_{ss} accounts for steam removed via vacuum pumps. The variation in steam pressure P_s within the shell is governed by:

$$\frac{dP_s}{dt} = \frac{R_s}{V} \left(\frac{dG_s}{dt} \right) (T_s + 273.15) \tag{2}$$

Here, R_s is the specific gas constant for steam, V is the effective gas volume, and T_s is the saturated steam temperature. The steam’s average enthalpy dynamics are described by:

$$\frac{dG_s H_s}{dt} = G_{st} H_{st} + G_{ost} H_{ost} - (G_c + G_{ss}) H_s \tag{3}$$

where H_s , H_{st} , and H_{ost} refer to the average enthalpy of steam inside the condenser, the turbine exhaust steam enthalpy, and any auxiliary steam input enthalpy, respectively.

2.2. *Mathematical Modeling of the Air Zone*

Non-condensable gases present in the condenser, such as air, significantly affect its thermal performance and pressure dynamics. The mass balance for air content G_a is defined by:

$$\frac{dG_a}{dt} = G_{vb} + G_n + G_g - G_a \tag{4}$$

where G_{vb} is the air inflow through the vacuum break valve, G_n is the air ingress from normal drainage, G_g accounts for seal leakages, and G_a is the air removal rate. Correspondingly, the variation in air pressure P_a is modeled as:

$$\frac{dP_a}{dt} = \frac{R_a}{V} \left(\frac{dG_a}{dt} \right) (T_s + 273.15) \quad (5)$$

with R_a being the specific gas constant for air. The overall absolute pressure P_c inside the condenser can then be expressed simply as the sum of steam and air partial pressures ($P_c = P_s + P_a$).

2.3. Mathematical Modeling of the Hot-Water Zone

The hot well, where condensate accumulates, has its own dynamics that are critical for overall mass balance. The hot well water level L_c can be calculated by $L_c = G_w / (\rho A_w)$, where G_w is the water mass, ρ is the water density, and A_w is the cross-sectional area of the hot well. The dynamics of water accumulation and enthalpy are governed by:

$$\frac{dG_w}{dt} = G_{gc} + G_{gp} - G_{wo} \quad (6)$$

$$\frac{dG_w H_w}{dt} = G_c H_{cw} + G_{gp} H_{gp} - G_{wo} H_w \quad (7)$$

where G_{gp} denotes the volume of oxygen expelled, G_{wo} is the water leaving the condenser, and H_{cw} and H_{gp} are enthalpies related to cooling water and exhaust gases, respectively.

2.4. Mathematical Modeling of the Cooling-Water Zone

The dynamic heat exchange occurring within the condenser tubes can be captured through an energy balance:

$$M_w C_w \frac{dT}{dt} = Q - Q_w \quad (8)$$

where M_w is the mass of cooling water, C_w is its specific heat, Q is the heat transferred from steam to cooling water, and Q_w is the heat carried away by the cooling water. The logarithmic mean temperature difference Δt_m required for evaluating heat transfer is computed as:

$$\Delta t_m = \frac{T - T_{cw}}{\ln \left(\frac{T_s - T_{cw}}{T_s - T} \right)} \quad (9)$$

In this model, T_{cw} and T refer to the inlet and outlet temperatures of the cooling water, respectively. Finally, a simplified model of the pressure dynamics under ideal gas assumptions, considering the condensation rate and volume changes, can be written as:

$$\frac{dP}{dt} = \frac{RT_c}{V} (F_s - F_c) \quad (10)$$

where F_s and F_c are the respective mass flow rates of steam inflow and condensate outflow.

2.5. System Parameters

The dynamic modeling of the shell-and-tube steam condenser system requires the adoption of specific thermodynamic and system parameters. The parameters reported in refs. [9,32,33] were considered in order to simulate the dynamic behavior of the nonlinear steam condenser system accurately. These parameter selections align with prior modeling studies and reflect typical operating conditions of industrial shell-and-tube steam condensers. They ensure that the developed mathematical model realistically captures the essential dynamics and nonlinearities of the system.

For compactness, the nonlinear steam condenser model described in Sections 2.1–2.4 may also be interpreted in a state-space-oriented form. In this representation, the overall system is written as $\dot{x}(t) = f(x(t), u(t))$, $y(t) = g(x(t), u(t))$ where $x(t)$ denotes the state vector collecting the main dynamic variables associated with the steam zone, air zone, hot-water zone, and cooling-water zone, $u(t)$ denotes the system input, and $y(t)$ denotes the measured output. In the present pressure regulation problem, the state vector is composed of the dominant thermodynamic variables introduced in Equations (1)–(10), whereas the output corresponds to the condenser pressure. Accordingly, the developed model may be viewed as a coupled nonlinear multi-state system in which mass and energy balances jointly determine the pressure evolution. This compact representation does not modify the physical model derived above; rather, it provides a unified summary of the model structure and highlights the coupled and nonlinear nature of the condenser dynamics considered in this study.

3. Atom Search Optimization Algorithm

Metaheuristic algorithms, inspired by natural phenomena, have demonstrated substantial success across a wide range of optimization problems [34–37]. Among them, the recently introduced atom search optimization (ASO) algorithm presents a novel approach that combines principles from molecular dynamics with heuristic search strategies [38]. ASO draws its core inspiration from the physical interactions observed among atoms, particularly the interplay of attractive and repulsive forces as governed by classical mechanics. In ASO, each atom represents a candidate solution within the search space. The behavior of the atoms is governed by two principal types of forces: interaction forces modeled by a modified Lennard-Jones potential, and constraint forces based on bond-length potentials [39]. The interaction forces facilitate exploration by allowing atoms to either attract or repel each other depending on their relative distances, while the constraint forces serve to maintain a structured movement toward the current best solution. This dual mechanism ensures a harmonious balance between global exploration and local exploitation, which is essential for avoiding premature convergence. At the heart of ASO lies Newton’s second law of motion, which relates the acceleration a_i of each atom i to the sum of the interaction force F_i and constraint force G_i divided by its mass m_i :

$$a_i = \frac{F_i + G_i}{m_i} \quad (11)$$

The interaction force between two atoms is mathematically derived from a modified Lennard-Jones potential, expressed as:

$$F_{ij}^l(t) = \eta(t) \left[2(h_{ij}(t))^{13} - (h_{ij}(t))^7 \right] \quad (12)$$

where $\eta(t)$ is a time-varying depth function controlling the balance between attraction and repulsion, and $h_{ij}(t)$ is a normalized interatomic distance factor. The position and velocity of each atom are iteratively updated according to the following relations:

$$v_i(t+1) = rand_i \cdot v_i(t) + a_i(t) \quad (13)$$

$$x_i(t+1) = x_i(t) + v_i(t+1) \quad (14)$$

where $rand_i$ is a random number in the interval $[0, 1]$, ensuring stochastic perturbations to the movement direction. A key adaptive mechanism in ASO is the gradual adjustment of

the number of neighboring atoms $K(t)$ considered during force calculations, decreasing over time according to:

$$K(t) = N - (N - 2)\sqrt{\frac{t}{T}} \quad (15)$$

where N is the total number of atoms, t is the current iteration, and T is the maximum number of iterations. This strategy enhances exploration in the early stages and exploitation in the later stages of the optimization process. The main parameters governing ASO behavior include α (the depth weight modulating the interaction strength), β (the multiplier weight regulating constraint forces), N (the population size of atoms), and T (the maximum number of iterations). Through the dynamic modulation of forces and adaptive neighborhood interactions, ASO successfully balances the competing needs for global search diversity and local convergence efficiency. Extensive benchmarking has demonstrated that ASO offers a competitive edge over several classic and emerging optimization methods, highlighting its potential for tackling complex, multimodal, and real-world engineering problems [40–47].

4. Proposed Hybrid Algorithm

Although the ASO algorithm has demonstrated strong global search capabilities, it shares a common shortcoming with many population-based methods: a diminished efficiency during the exploitation phase. As the optimization advances, ASO tends to lose its ability to effectively concentrate the search around the most promising regions, leading to slower convergence [48]. To overcome this limitation, we introduce a hybrid version of ASO, referred to as the hybrid adaptive gbest-guided atom search optimization and pattern search (hGASO-PS) algorithm, which integrates an adaptive guidance mechanism [49] centered on the global best solution and performs pattern search mechanism [50] to further improve the solution. To adaptively balance the global and local search behaviors, we integrate a gbest-guided mechanism into the standard ASO such that the velocity of each atom is updated using the following formulation:

$$v_i(t+1) = rand_i \cdot v_i(t) + c_1 \cdot a_i(t) + c_2 \cdot (gbest - x_i(t)) \quad (16)$$

Here, c_1 and c_2 are adaptive coefficients controlling the influence of acceleration and attraction towards the global best, respectively. Their values evolve over iterations according to:

$$c_1 = \left(\frac{-2t^3}{T^3} \right) + 2, \quad c_2 = \left(\frac{2t^3}{T^3} \right) \quad (17)$$

These dynamic parameters ensure that early iterations emphasize exploration ($c_1 > c_2$), while the later stages prioritize exploitation by increasing the weight of the global best influence ($c_2 > c_1$). In the proposed hGASO-PS framework, the principal algorithmic quantities are determined in a straightforward and adaptive manner. The current best fitness value is not prescribed in advance; rather, it is obtained iteratively as the minimum objective function value achieved by the population up to the current iteration. Similarly, the iteration index t is simply the running counter of the optimization process, whereas T denotes the predefined maximum number of iterations and serves as the stopping limit of the global search stage. Therefore, quantities such as the best fitness and the current global best solution are updated automatically during the search, while the adaptive coefficients in Equation (17) are calculated directly from the normalized iteration progress (t/T). In this way, the parameter adaptation mechanism does not require additional manual tuning and naturally shifts the search behavior from exploration in the early iterations to exploitation in the later ones.

While ASO and its adaptive variant are effective in global search, they may struggle to refine solutions in the vicinity of the optimum. To address this, the pattern search (PS) mechanism [51] (shown in Figure 2) is employed as a local optimizer. It operates by generating mesh points in four principal directions: $[1, 0]$, $[0, 1]$, $[-1, 0]$, and $[0, -1]$. These directions are iteratively expanded or contracted depending on the success of the search.

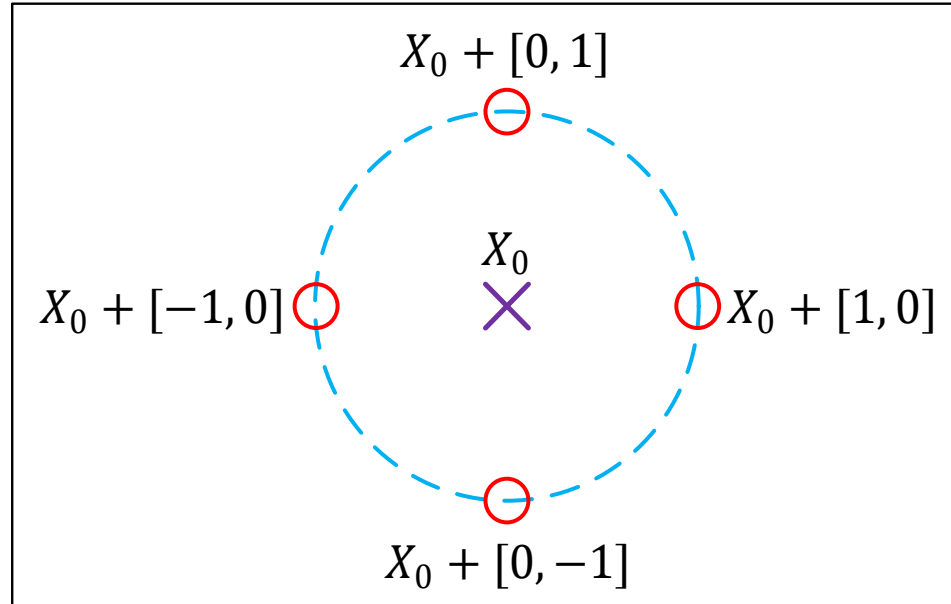


Figure 2. The process of the pattern search mechanism.

Let X_k be the current solution. The pattern mesh at iteration k is defined by:

$$X_k = \Delta_k \cdot d, \quad d \in \{[1, 0], [0, 1], [-1, 0], [0, -1]\} \tag{18}$$

If a better solution is found, Δ_k is increased (expansion); otherwise, it is reduced (contraction), guiding the search toward optimal regions. This mechanism enhances the exploitation phase, ensuring precise convergence [52]. In the context of the above mechanisms, the hybrid algorithm proceeds in two stages (as detailed in Figure 3):

1. Global search with adaptive ASO: The population of candidate solutions (atoms) evolves using the adaptive gbest-guided ASO described above. The global search is continued until a stopping criterion or satisfactory convergence is achieved.
2. Local exploitation via PS: The best solution obtained from the ASO stage is used to initialize the PS algorithm. This second stage refines the solution locally by exploring the immediate neighborhood using deterministic mesh patterns.

This sequential combination allows the algorithm to effectively explore the global landscape and then concentrate search efforts near the most promising region.

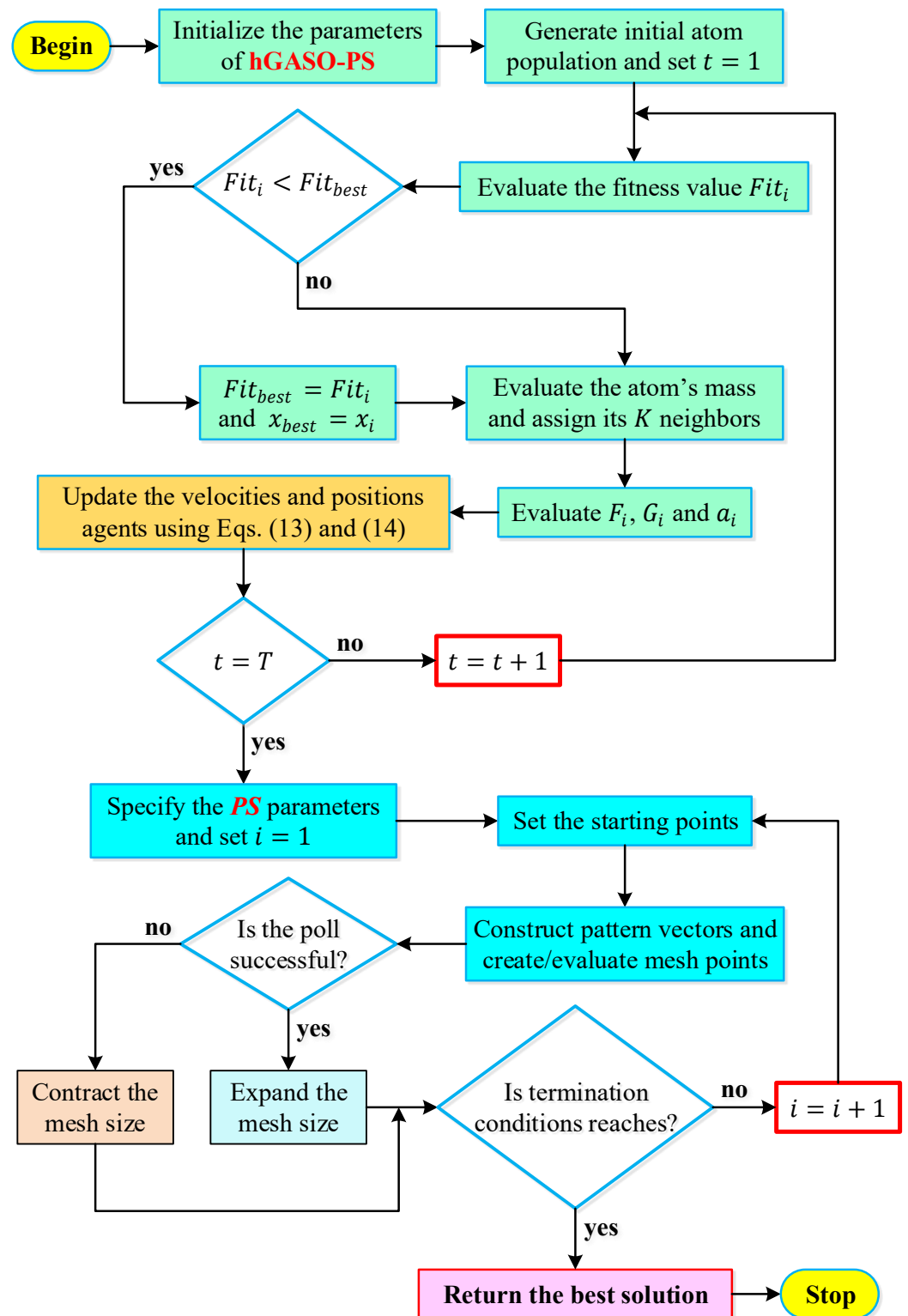


Figure 3. Flowchart of hGASO-PS algorithm.

5. Novel Control Approach

5.1. Cascaded Softsign Function-Based PID Controller

To enhance the robustness and adaptability of control in highly nonlinear systems such as steam condensers, a novel control approach (termed the cascaded softsign function-based PID (CSoft-PID) controller) is proposed. This controller builds upon the classical PID framework [10] but introduces a nonlinear shaping mechanism via a softsign function to

improve transient response and prevent aggressive control actions. The conventional PID structure used in this work is defined in the Laplace domain as:

$$C_{PID}(s) = K_P + \frac{K_I}{s} + \frac{Ns}{s+N}K_D \quad (19)$$

This form incorporates a filtered derivative term using the parameter N , which helps to mitigate noise sensitivity—a known limitation of pure derivative action. While this controller effectively combines proportional (K_P), integral (K_I), and derivative (K_D) dynamics, its behavior remains linear with respect to the error signal. To enhance its nonlinear response characteristics, a softsign transformation [28] is applied to the error before it feeds into the control law. The softsign function is defined as:

$$\text{Softsign}(x) = \frac{x}{1+|x|} \quad (20)$$

This function introduces a smooth, saturating nonlinearity that compresses the control signal as the input magnitude increases, thereby allowing high sensitivity near the setpoint and bounded responses during large disturbances.

While nonlinear error-shaping mechanisms based on functions such as sigmoid, hyperbolic tangent, and saturation have been explored in previous studies, the softsign function provides several distinct properties that make it particularly suitable for practical control applications. Unlike sigmoid or tanh functions, which rely on exponential terms, the softsign function possesses a rational polynomial form. This structure produces a smooth and gradual saturation characteristic while maintaining a relatively simple computational structure.

From a control perspective, this property offers three important advantages. First, the softsign transformation limits the magnitude of the error signal in a continuous and bounded manner, preventing excessively aggressive control actions during large transient deviations. Second, the function maintains an approximately linear slope in the vicinity of the origin, which preserves high sensitivity near the setpoint and enables accurate steady-state regulation. Third, the absence of exponential operations reduces computational complexity and improves numerical robustness, which is advantageous for real-time implementation in industrial control systems.

Therefore, the softsign function provides a balanced nonlinear shaping mechanism that simultaneously maintains sensitivity near the operating point and suppresses excessive actuation under large disturbances. In the proposed controller architecture, this transformation is implemented in a cascaded structure together with two adjustable gains, allowing the degree of nonlinear shaping to be flexibly tuned during the optimization process.

As shown in Figure 4, the proposed CSoft-PID controller cascades this nonlinear transformation after a linear scaling stage. The error signal $e(t)$ is first scaled by a gain G_1 , yielding:

$$l(t) = G_1 \times e(t) \quad (21)$$

This signal $l(t)$ is then passed through the softsign function and further scaled by a second gain G_2 , resulting in the nonlinear control input:

$$v(t) = G_2 \times \text{Softsign}(l(t)) = G_2 \times \text{Softsign}(G_1 \times e(t)) = G_1 \times G_2 \times \frac{e(t)}{1+|G_1 \times e(t)|} \quad (22)$$

This cascaded arrangement forms the core of the CSoft-PID controller, where the input of the PID controller ($v(t)$) is a nonlinear transformation of the error signal, modulated by tunable gains G_1 and G_2 . The purpose of this structure is to retain the intuitive nature of

PID control, while introducing a nonlinear correction layer that dynamically adjusts the response intensity based on the magnitude of the error.

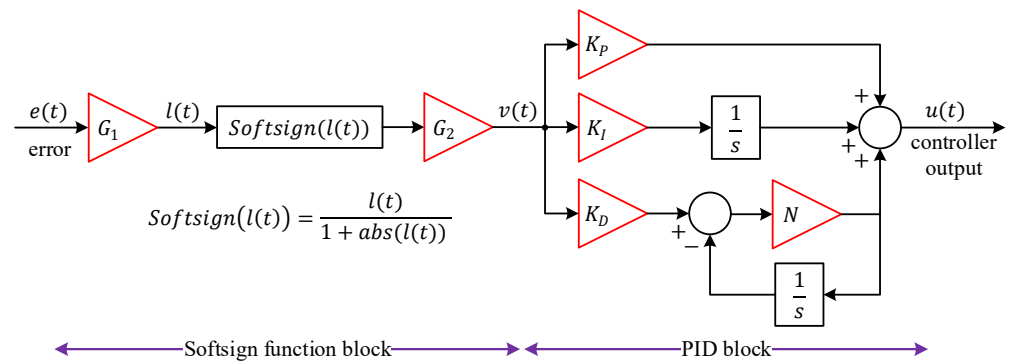


Figure 4. Block diagram of CSoft-PID controller.

Figure 4 visually illustrates the architecture of this controller. The error signal enters a gain block G_1 , then passes through a softsign function, and is finally scaled by G_2 . This processed signal, which reflects a shaped version of the error, is then used within the broader PID control loop as an input, enhancing stability and mitigating the risk of overshoot or oscillations in dynamic scenarios. In summary, the CSoft-PID controller offers a practical and computationally efficient enhancement over conventional PID designs. By cascading a nonlinear transformation that adapts to error magnitude, the controller achieves smoother transient performance, better handling of nonlinear dynamics, and more graceful saturation behavior, making it particularly well-suited for complex industrial systems such as steam condensers.

5.2. Definition of Optimization Problem

To ensure high-performance control of the nonlinear steam condenser system, the parameters of the proposed CSoft-PID controller must be finely tuned. This tuning process is formulated as a constrained optimization problem in which the goal is to minimize a predefined objective function that captures the controller's effectiveness in reducing pressure tracking error over time. The objective function selected for this study is the integral of time-weighted absolute error (ITAE), which penalizes both the magnitude of the control error and its duration. This function is defined as [53]:

$$ITAE = \int_{t_1}^{t_2} (t - t_1) |e(t)| dt \quad (23)$$

where $e(t)$ denotes the instantaneous error signal, calculated as the difference between the desired pressure setpoint and the actual output of the condenser system. In this study, the evaluation interval of the ITAE objective function is selected as $[t_1 = 10 \text{ s}, t_2 = 50 \text{ s}]$. The lower bound $t_1 = 10 \text{ s}$ corresponds to the instant at which the step change in the condenser pressure reference is introduced, ensuring that the optimization process focuses directly on the transient response of the closed-loop system rather than the pre-disturbance steady-state condition. The upper bound $t_2 = 50 \text{ s}$ is chosen because this duration is sufficient for all examined controller configurations to complete their dominant transient behavior and approach steady-state operation. Therefore, the selected interval captures the main dynamic characteristics of interest, including overshoot, oscillations, and settling behavior, whereas the tracking error outside this range remains negligible due to steady-state regulation. The ITAE criterion is particularly suitable for pressure regulation applications, as it

emphasizes fast settling with minimal sustained error, thereby promoting both accuracy and responsiveness.

To rigorously evaluate the controller under dynamic conditions, a pressure setpoint change is introduced during the simulation. Specifically, the reference pressure P is initially held at 90 kPa, then increased to 95 kPa at time $t_1 = 10$ s. This step change allows the assessment of the controller's performance during both steady-state and transient periods. The optimization process also involves adjusting the following six control parameters: K_P , K_I , K_D , N , G_1 , and G_2 . These parameters are subject to the following constraints to ensure safe and realistic operation of the controller: $1 \leq K_P \leq 100$, $0.1 \leq K_I \leq 10$, $1 \leq K_D \leq 100$, $5 \leq N \leq 1000$, $0.1 \leq G_1 \leq 10$, and $0.1 \leq G_2 \leq 10$. These bounds were chosen based on preliminary experiments and control engineering heuristics to maintain system stability and avoid excessively aggressive control actions. The optimization algorithm seeks to determine the optimal set of these six parameters that minimizes the ITAE objective function, thereby achieving accurate, fast, and stable pressure regulation in the shell-and-tube steam condenser system.

5.3. Application of hGASO-PS Algorithm

The proposed hybrid algorithm, hGASO-PS, plays a central role in fine-tuning the control parameters of the newly developed CSoft-PID controller to ensure optimal performance within the nonlinear dynamics of the steam condenser system. As detailed earlier, hGASO-PS integrates the global exploration strength of the adaptive gbest-guided ASO algorithm with the local search precision of the PS technique. This hybridization ensures that both global optimality and local refinement are achieved in the search for the best controller settings.

The complete implementation strategy is illustrated in Figure 5, which outlines the interconnection between the nonlinear condenser model, the optimization framework, and the controller structure. As shown, the process begins with initializing the hGASO-PS algorithm, where an initial population of candidate solutions (each representing a distinct set of controller parameters) is randomly generated within the defined bounds. Each candidate solution is evaluated based on the ITAE objective function defined in Section 5.2. This evaluation involves simulating the nonlinear condenser system's dynamic response using the candidate CSoft-PID controller settings and computing the integral of time-weighted absolute error resulting from a predefined pressure setpoint change.

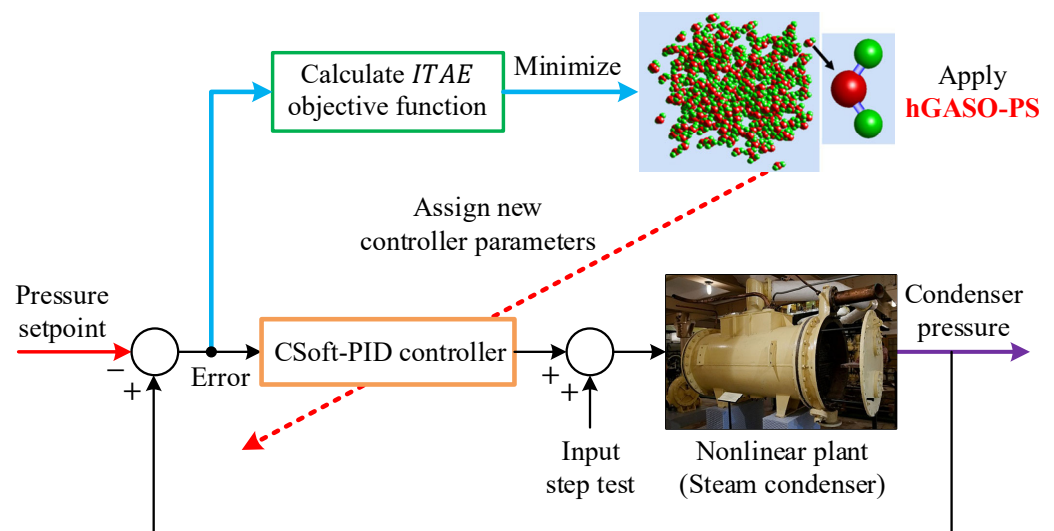


Figure 5. The implementation of hGASO-PS tuned novel CSoft-PID controller to nonlinear steam condenser system.

Within the hGASO-PS framework, the ASO mechanism first guides the population using atom-inspired dynamics and adaptive global best attraction. The gbest-guided approach enables the algorithm to gradually shift from global search to a more refined local regions as iterations progress. Once a sufficiently promising solution is identified, the PS module is invoked to fine-tune this solution further. This phase performs a localized search around the best solution using mesh-based directional probes, aiming to minimize the ITAE value even further. This two-phase optimization loop continues until the stopping condition is satisfied (by reaching the maximum number of iterations). The outcome is the optimal parameter set for the CSoft-PID controller, which is then embedded within the closed-loop system for final performance verification. In essence, the application of hGASO-PS to the nonlinear condenser system enables automated and intelligent calibration of the controller. This hybrid algorithm not only ensures robust convergence to high-quality solutions but also facilitates reliable pressure regulation with reduced steady-state error, faster settling, and smoother transient behavior.

6. Simulation Results

6.1. Statistical Test and Evolution of Objective Function

To assess the robustness and consistency of the proposed hGASO-PS-based CSoft-PID controller, a comprehensive comparative evaluation was carried out using a statistical approach over 30 independent runs. For a fair comparison, all algorithms were executed under the same optimization framework, using the identical objective function defined in Equation (23), the same controller parameter bounds, a population size of 40, and a maximum of 100 iterations. In all cases, the initial candidate solutions were randomly generated within the same predefined search intervals of the controller parameters. Furthermore, the internal parameters of the benchmark algorithms were not additionally retuned for the present problem; instead, the default parameter settings recommended in their original studies were adopted. For comparative purposes, the recent and good-performing algorithms of ASO [38], Newton–Raphson-based optimizer (NRBO) [54], honey badger algorithm (HBA) [55], and sine cosine algorithm (SCA) [56] were used.

The results of the statistical performance across all algorithms are presented in Figure 6 and Table 1. The boxplot in Figure 6 visually illustrates the distribution of ITAE values obtained from 30 independent runs for each algorithm. As observed, the proposed hGASO-PS algorithm not only achieves the lowest median ITAE but also exhibits a narrow interquartile range, indicating its strong consistency and stability across multiple runs. In contrast, other algorithms such as the standard ASO, NRBO, HBA, and SCA show wider spreads and higher median values, signifying either less accurate convergence or more variable outcomes.

Table 1. Comparative numerical values for statistical performance.

Algorithm	Mean	Standard Deviation	Best	Worst
hGASO-PS	2.2746	0.0934	2.1608	2.5607
ASO	2.8189	0.0801	2.6986	2.9822
NRBO	3.0439	0.0977	2.9029	3.2664
HBA	3.2306	0.0918	3.0650	3.4380
SCA	3.4423	0.1695	3.2831	4.1080

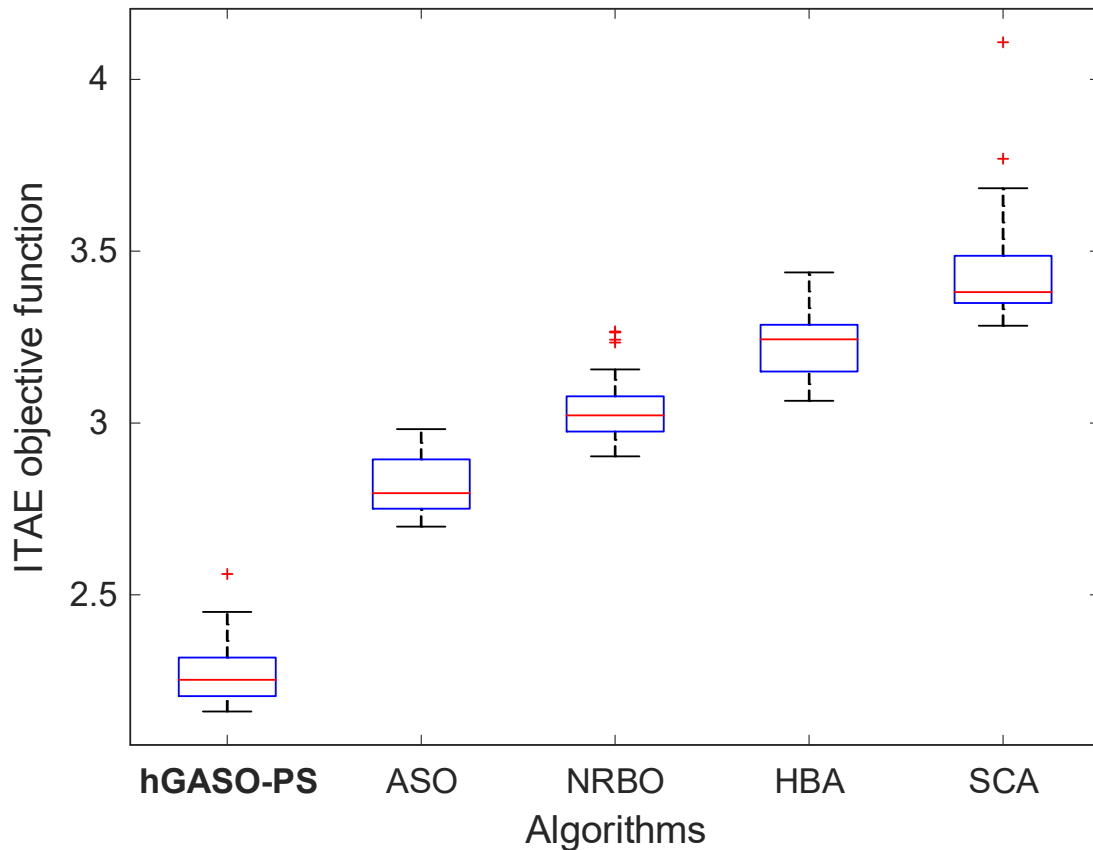


Figure 6. Boxplot evaluation based on the minimization of the ITAE objective function value.

The numerical values further confirm this observation. As summarized in Table 1, the hGASO-PS algorithm yields the lowest mean ITAE value of 2.2746 with a standard deviation of 0.0934. Its best recorded ITAE was 2.1608, while the worst remained at 2.5607 (still outperforming the average performance of all competing methods). The second-best performer, ASO, had a mean ITAE of 2.8189 and a higher worst-case value of 2.9822. The performance degradation is more noticeable with algorithms like HBA and SCA, whose worst-case results reached up to 3.4380 and 4.1080, respectively.

To further explore convergence behavior, Figure 7 presents the best convergence curves of each algorithm. The curves illustrate how the objective function value evolves over iterations. Here, hGASO-PS stands out with a rapid initial decline in ITAE, followed by a smooth and steady convergence trend, ultimately reaching a lower final error than all other methods. This demonstrates the effectiveness of the hybrid mechanism in balancing exploration and exploitation throughout the optimization process. In contrast, some algorithms like NRBO and SCA show slower descent and earlier stagnation, suggesting that they may be more prone to premature convergence.

Complementing the statistical and convergence analysis, Table 2 lists the optimal parameter sets of the CSoft-PID controller obtained by each algorithm. The hGASO-PS-tuned controller features notably larger proportional and derivative gains compared to its competitors, which likely contributed to its faster transient response. Additionally, the gains associated with the nonlinear shaping structure reflect a more moderate but stable shaping effect, helping the controller avoid excessive actuation and maintain robust performance. In summary, the statistical test and objective function evolution analysis clearly indicate that the hGASO-PS algorithm not only provides superior control accuracy but also maintains high reliability across multiple trials. These findings validate the

algorithm’s effectiveness in tuning the CSoft-PID controller for dynamic pressure regulation in nonlinear condenser environments.

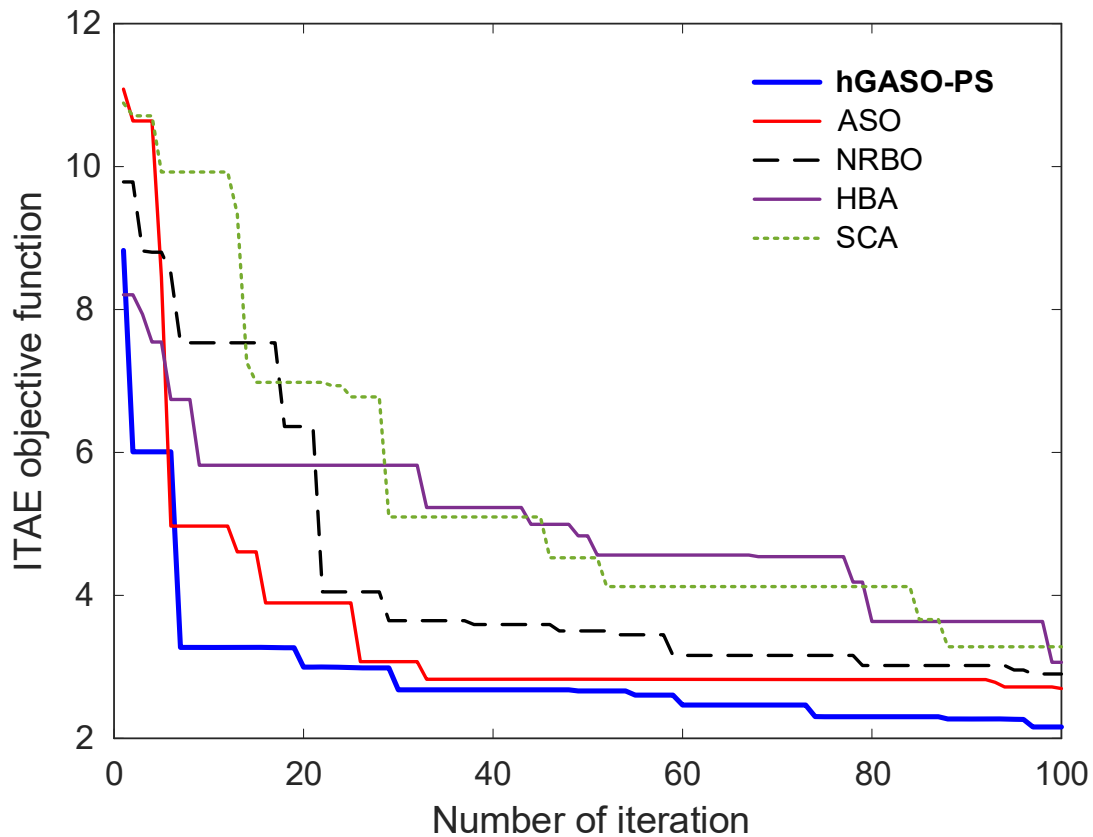


Figure 7. Comparative convergence curves demonstrating the minimization of ITAE with respect to iterations.

Table 2. Optimal parameters of CSoft-PID controller obtained by different algorithms.

Algorithm	K_P	K_I	K_D	N	G_1	G_2
hGASO-PS	80.1191	1.5810	75.3387	573.5719	0.2767	6.7309
ASO	53.6933	1.2813	62.0966	516.6798	0.4211	6.2016
NRBO	89.2304	2.7917	96.3650	585.0400	0.4215	2.8376
HBA	43.8164	2.4606	64.0248	756.7654	1.1601	2.0134
SCA	58.9604	4.3778	75.2959	880.6523	1.6108	1.0585

6.2. Closed-Loop Response

To further validate the performance of the proposed hGASO-PS-based CSoft-PID controller under dynamic operating conditions, a step-change simulation was conducted on the nonlinear steam condenser system. The goal was to evaluate how effectively each controller configuration regulates the condenser pressure in response to a reference input disturbance. As illustrated in Figure 8, the simulation begins with an initial pressure setpoint of 90 kPa, which is increased to 95 kPa at 10 s. The Figure depicts the step response of the condenser pressure under five different configurations: the proposed hGASO-PS-based CSoft-PID and those tuned by ASO, NRBO, HBA, and SCA.

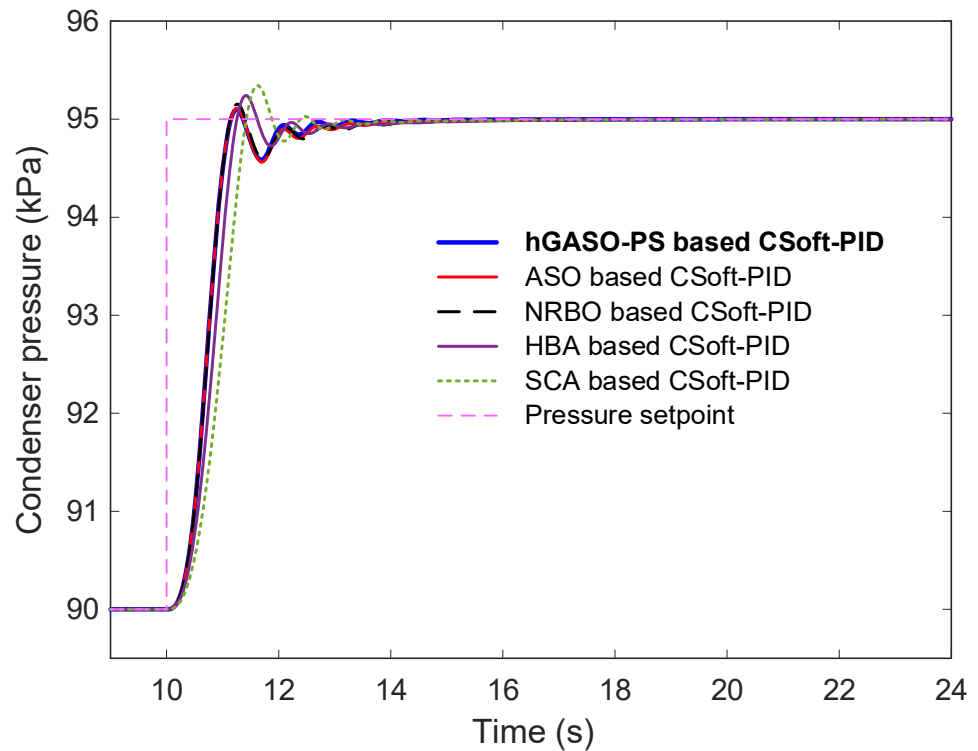


Figure 8. Step response showing the change in condenser pressure from 90 kPa to 95 kPa at $t = 10$ s.

A visual inspection of the step responses reveals that the hGASO-PS-based controller delivers the fastest and smoothest tracking with minimal overshoot and rapid settling. A more detailed perspective is presented in Figure 9, which zooms in on the transient region surrounding the step change. In this closer view, the superiority of the hGASO-PS-based CSoft-PID controller becomes even more evident. Unlike other controllers, which exhibit noticeable overshoots and longer transient tails, the proposed controller responds swiftly and stabilizes the system output without oscillatory behavior. To quantitatively support these observations, Table 3 presents the key transient performance metrics derived from the closed-loop simulations. These include:

- Normalized rise time (n_{rt}): time taken to rise from 10% to 90% of the final value;
- Normalized rise time (n_{st}): time required for the output to remain within $\pm 2\%$ of the final value;
- Normalized rise time (n_{os}): the maximum peak beyond the steady-state value expressed as a percentage;
- Normalized rise time (n_{pt}): the time at which the peak response occurs.

Table 3. Numerical transient performance of different algorithms.

Algorithm	n_{rt} (s)	n_{st} (s)	n_{os} (%)	n_{pt} (s)
hGASO-PS	0.6180	12.5096	1.9823	11.2477
ASO	0.6190	13.0096	2.1658	11.2508
NRBO	0.6192	13.2438	3.0758	11.2647
HBA	0.7042	12.7072	4.8169	11.4175
SCA	0.8154	12.8445	6.8440	11.6250

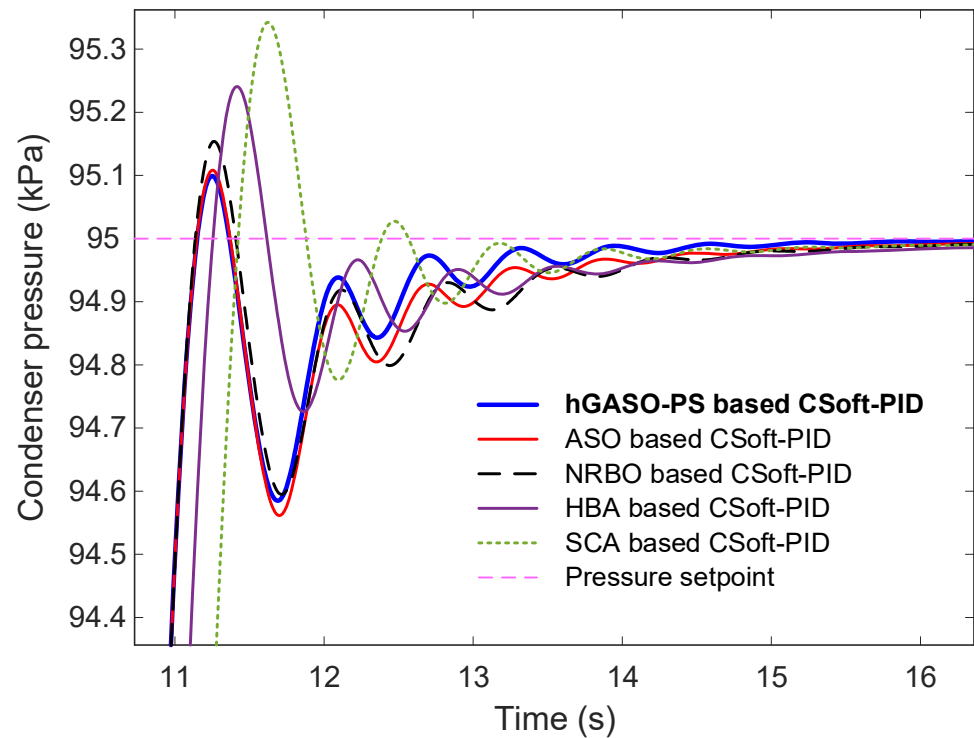


Figure 9. Zoomed view of Figure 8.

Among all tested controllers, the hGASO-PS-based CSoft-PID demonstrates the lowest normalized overshoot (1.9823%) and the fastest normalized settling time (12.5096 s), while maintaining a minimal normalized rise time and normalized peak time. These metrics reflect its ability to deliver rapid and stable responses with minimal deviation from the target value. Although the ASO-based controller achieves comparable normalized rise and peak times, it still lags behind in terms of normalized overshoot and settling precision. Controllers based on HBA and SCA, in particular, display significantly larger normalized overshoots and delayed responses, underscoring their limitations in handling the nonlinearities of the system effectively. Overall, the closed-loop performance results reaffirm the superior dynamic behavior of the proposed hGASO-PS-tuned CSoft-PID controller. It consistently achieves better transient characteristics, making it a promising solution for real-world steam condenser applications that demand fast, precise, and reliable pressure regulation.

6.3. Comparison with Reported Studies

To rigorously assess the efficacy of the proposed hGASO-PS-based CSoft-PID controller, its performance was compared against several state-of-the-art controllers reported in the literature. These include optimization-based proportional–integral (PI), fractional-order PID (FOPID), and cascaded PI-PDN controllers designed using various advanced metaheuristic algorithms such as the gray wolf optimizer (GWO) [33], particle swarm optimization (PSO) [33], gazelle optimization algorithm (GOA) and its logarithmic spiral version (Ls-GOA) [57], enhanced cooperation search (en-CSA) [32], rime optimizer [32], sinh-cosh optimizer (SCHO) [58], aquila optimizer (AO) [58], electric eel foraging optimizer (EEFO) [59], quadratic interpolation optimizer (QIO) [59], golden eagle optimizer (GEO) [59], and slime mold algorithm (SMA) [59]. These methods are listed in Table 4. The comparative evaluations are categorized into three groups based on the type of controller design. These comparisons are made under identical simulation scenarios, particularly

involving a step change in the pressure setpoint from 90 kPa to 95 kPa, to ensure consistency across all assessments.

Table 4. Comparative numerical performance analyses with respect to reported approaches in the literature.

Method No.	Reference	Algorithm	Control Scheme
1	[33]	GWO	PI
2	[33]	PSO	PI
3	[57]	GOA	PI
4	[57]	Ls-GOA	PI
5	[32]	en-CSA	FOPID
6	[32]	RIME	FOPID
7	[58]	SCHO	FOPID
8	[58]	AO	FOPID
9	[59]	EEFO	Cascaded PI-PDN
10	[59]	QIO	Cascaded PI-PDN
11	[59]	GEO	Cascaded PI-PDN
12	[59]	SMA	Cascaded PI-PDN

6.3.1. Comparison with Reported PI-Based Approaches

As shown in Figure 10, the hGASO-PS-tuned CSoft-PID controller significantly outperforms the PI controllers optimized using GWO, PSO, GOA, and Ls-GOA in terms of transient response. The step response profile demonstrates faster settling, lower overshoot, and improved tracking accuracy. Numerical results in Table 5 confirm these observations. The proposed controller achieved the lowest overshoot (1.9823%), fastest settling time (12.5096 s), and shortest rise time (0.6180 s). In comparison, even the best-performing PI approach (GWO-based) showed a settling time of 19.8228 s and an overshoot of 21.0680%, which is more than 10 times higher than that of the CSoft-PID controller.

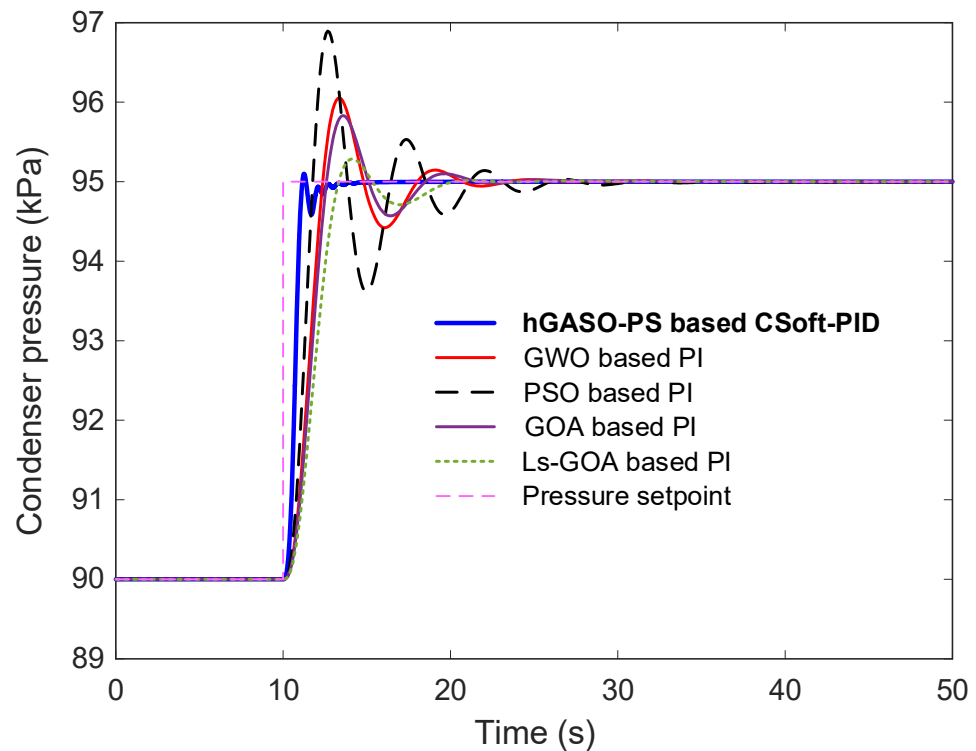


Figure 10. Step response of the proposed hGASO-PS-based CSoft-PID with respect to reported PI-based approaches.

Table 5. Comparative numerical performance evaluation with respect to reported PI-based approaches.

Control Approach	n_{rt} (s)	n_{st} (s)	n_{os} (%)	n_{pt} (s)
hGASO-PS-based CSoft-PID	0.6180	12.5096	1.9823	11.2477
GWO-based PI	1.4436	19.8228	21.0680	13.3639
PSO-based PI	1.0513	24.9424	37.8753	12.6667
GOA-based PI	1.5929	19.7733	16.6180	13.5921
Ls-GOA-based PI	2.0267	18.9174	5.7279	14.1223

6.3.2. Comparison with Reported FOPID-Based Approaches

The next set of comparisons, presented in Figure 11 and Table 6, includes FOPID controllers optimized using en-CSA, RIME, SCHO, and AO algorithms. Despite the increased flexibility offered by fractional-order structures, the proposed integer-order CSoft-PID controller outperformed all reported FOPID controllers in terms of rise time, settling time, and overshoot. For instance, the best among the FOPID controllers (en-CSA-based) resulted in an overshoot of 8.7070% and a settling time of 16.5104 s, which still falls short of the performance achieved by the hGASO-PS-based controller.

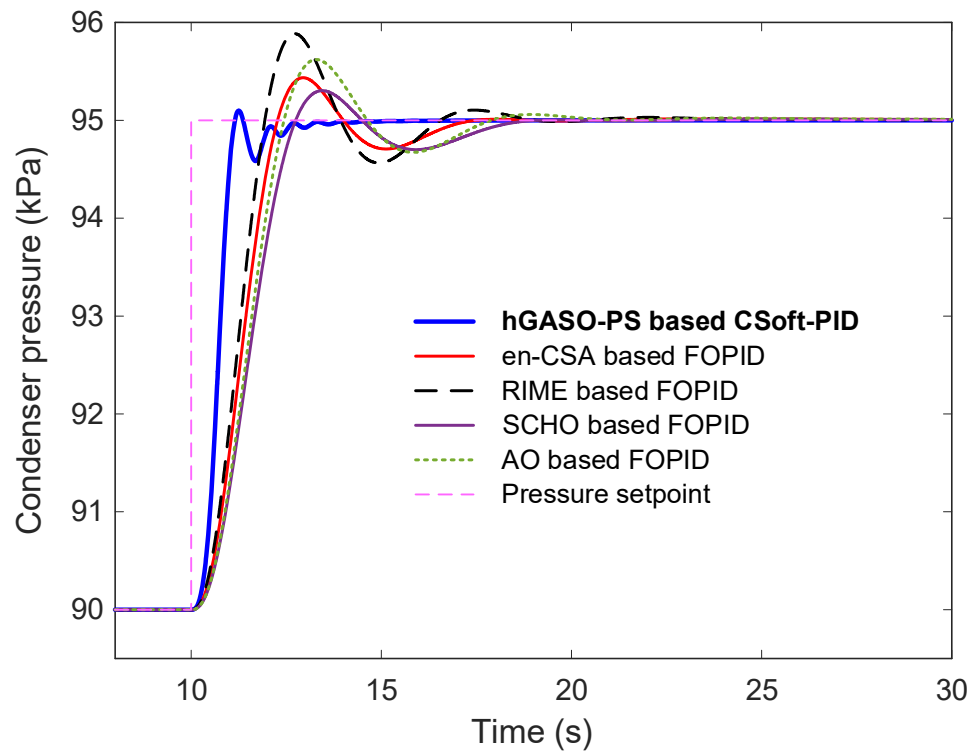


Figure 11. Step response of the proposed hGASO-PS-based CSoft-PID with respect to reported FOPID-based approaches.

Table 6. Comparative numerical performance evaluation with respect to reported FOPID-based approaches.

Control Approach	n_{rt} (s)	n_{st} (s)	n_{os} (%)	n_{pt} (s)
hGASO-PS-based CSoft-PID	0.6180	12.5096	1.9823	11.2477
en-CSA-based FOPID	1.4095	16.5104	8.7070	12.9427
RIME-based FOPID	1.2115	17.6610	17.7156	12.7197
SCHO-based FOPID	1.7037	17.6635	6.0647	13.4467
AO-based FOPID	1.5232	17.2855	12.4207	13.2887

6.3.3. Comparison with Reported Cascaded PI-PDN-Based Approaches

The final set of comparisons targets cascaded PI-PDN controllers optimized with EEFO, QIO, GEO, and SMA algorithms. As illustrated in Figure 12 and the zoomed view in Figure 13, the proposed controller again shows superior performance, achieving faster settling with less overshoot and reduced oscillatory behavior. From Table 7, the proposed controller maintained the lowest overshoot (1.9823%) compared to 2.5609% (EEFO), 3.8836% (QIO), 4.6208% (GEO), and 7.9315% (SMA). While some cascaded structures like SMA exhibited slightly faster rise times, they suffered from significant overshoot and longer settling durations. Lastly, Figure 14 visualizes the final ITAE objective values attained by each controller. The hGASO-PS-tuned CSoft-PID controller clearly achieves the lowest ITAE value among all compared approaches, further reinforcing its efficiency and robustness in regulating the nonlinear steam condenser system.

Table 7. Comparative numerical performance evaluation with respect to reported cascaded PI-PDN-based approaches.

Control Approach	n_{rt} (s)	n_{st} (s)	n_{os} (%)	n_{pt} (s)
hGASO-PS-based CSoft-PID	0.6180	12.5096	1.9823	11.2477
EEFO-based PI-PDN	0.6451	13.1799	2.5609	12.3907
QIO-based PI-PDN	0.6216	13.5744	3.8836	12.6384
GEO-based PI-PDN	0.6815	14.1196	4.6208	11.4138
SMA-based PI-PDN	0.5937	13.9776	7.9315	11.2872

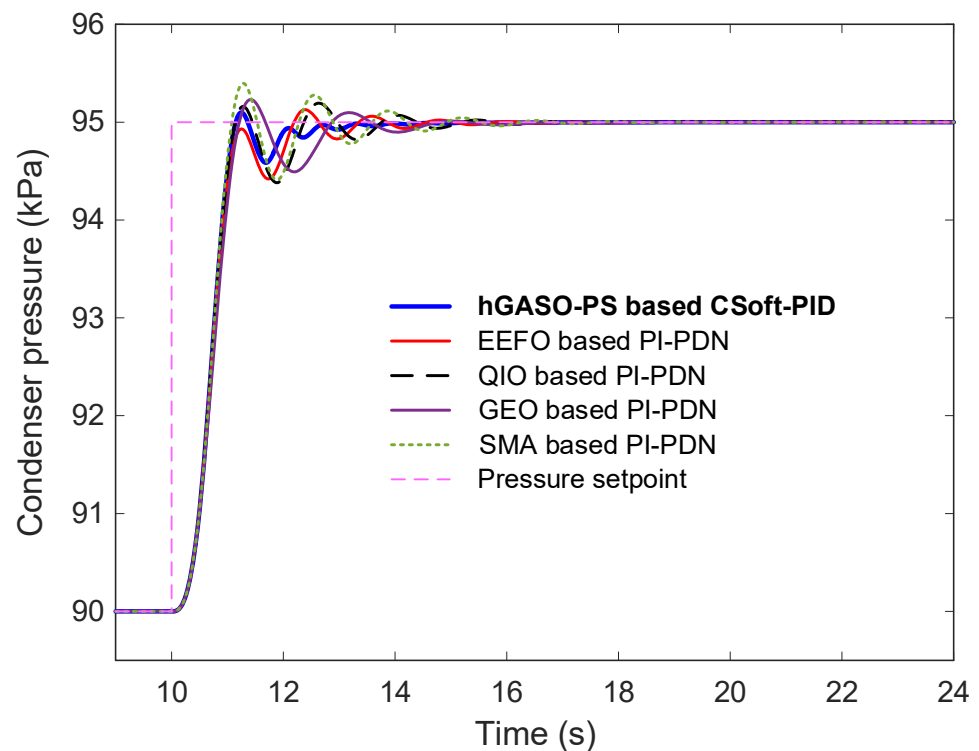


Figure 12. Step response of the proposed hGASO-PS-based CSoft-PID with respect to reported cascaded PI-PDN-based approaches.

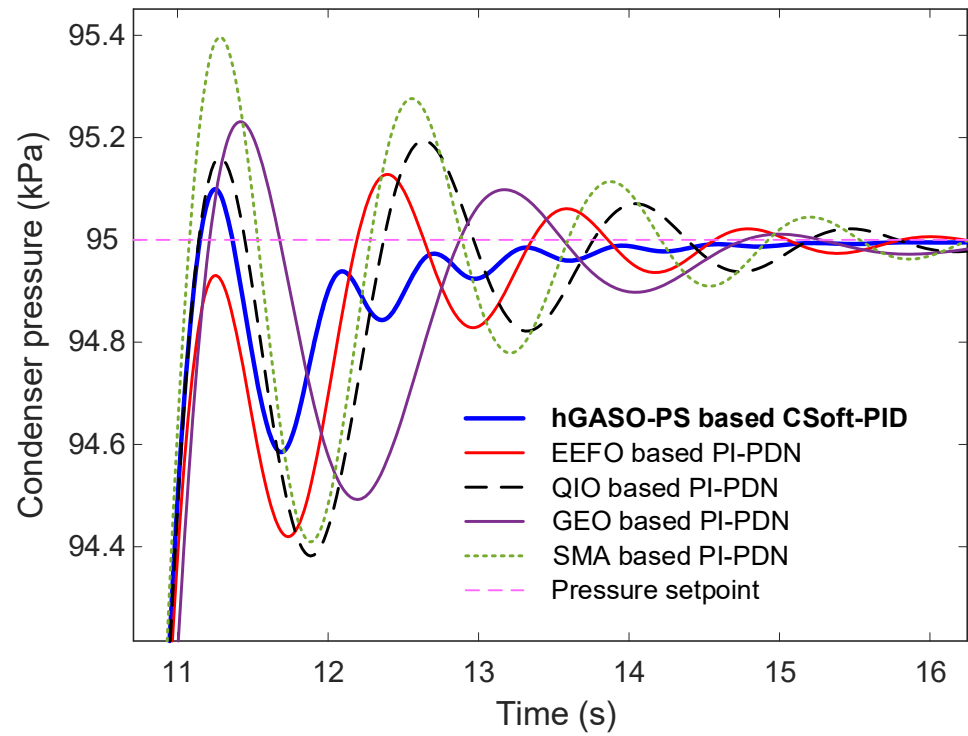


Figure 13. Zoomed view of Figure 12.

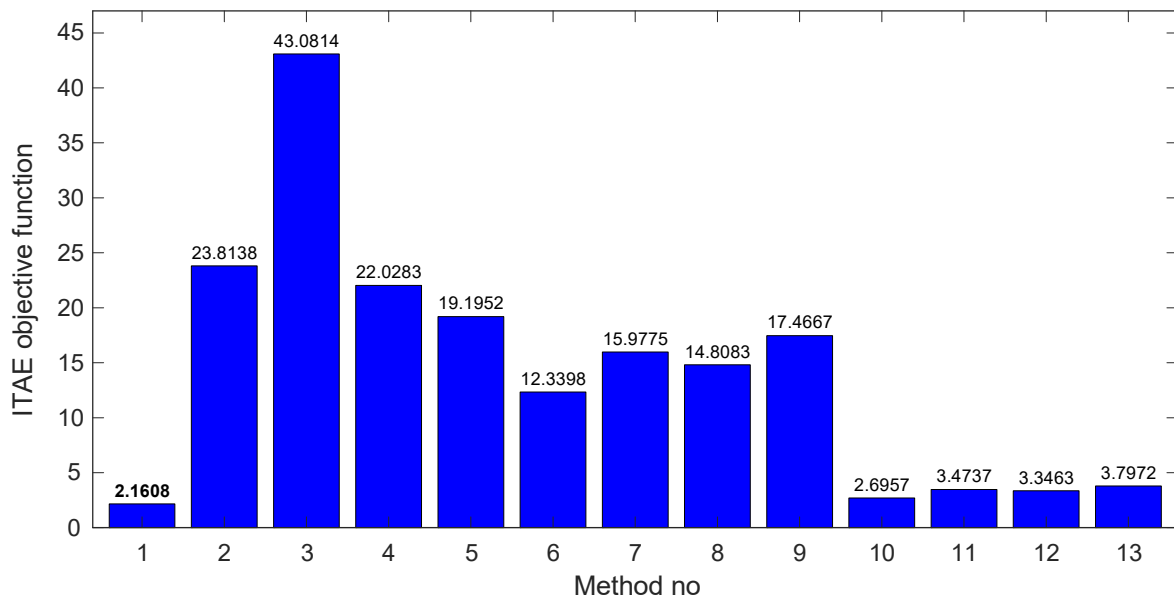


Figure 14. Comparison of ITAE objective function values for different reported approaches.

6.4. Real-Time Implementation of the CSoft-PID Controller

To further support the practical applicability of the proposed control strategy, a simplified real-time experimental validation was conducted. Since direct access to an industrial steam condenser system was not available, a laboratory-scale test platform was employed to demonstrate the real-time feasibility and robustness of the proposed CSoft-PID controller under representative dynamic conditions. The developed experimental setup is illustrated in Figure 15. The platform is centered around a permanent magnet brushed DC (PMDC) motor system, which is widely used as a benchmark for evaluating control strategies due to its nonlinear characteristics and sensitivity to disturbances. The control algorithm was

implemented on a DSP-based embedded system (TMS320F28335), which handled real-time signal acquisition, controller execution, and command generation.

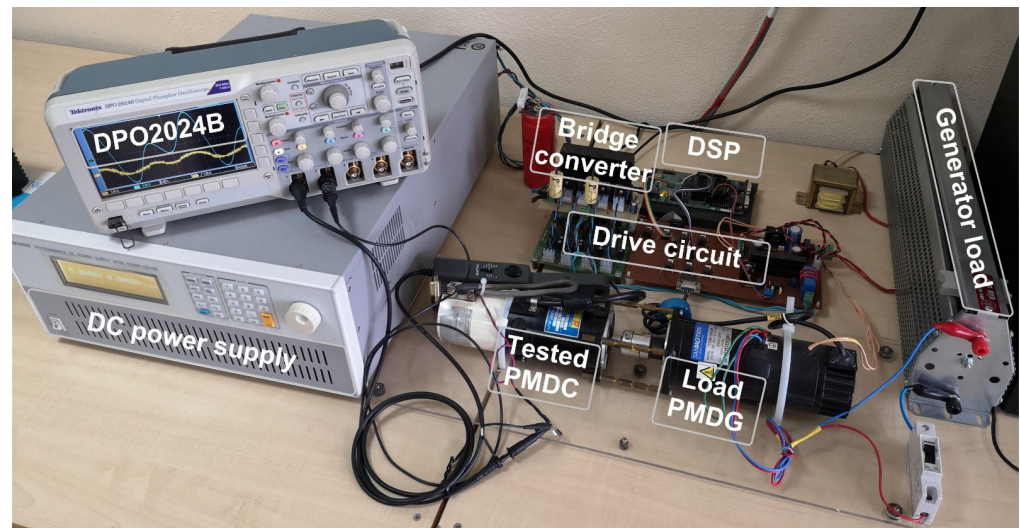


Figure 15. Test platform for speed regulation.

Commercially available TMS320F28335 (TI) digital signal processor (DSP) is used for managing the system, receiving feedback signals such as position and current from the PMDC motor, and sending commands to the bridge converter that supplies the PMDC motor. The PMDC motor model under control is Sanyo Denki R730T-042EL7. The generator model is Sanyo Denki T730B-569EL8N, which is coupled to the PMDC motor in order to apply external torque disturbances when required. Sampling time for controlling the motor armature current and speed was set to $13.33 \mu\text{s}$ and $500 \mu\text{s}$, respectively. The system speed response is accurately acquired through the output voltage of a tachogenerator with a voltage constant of 7.4 V/krpm , and this, in addition to the motor current, is collected by a Tektronix DPO2024 oscilloscope. The PMDC motor nominal parameters are included in Table 8.

Table 8. PMDC motor nominal parameters.

Description	Value
Rated power	300 W
Rated armature current	4.8 A
Rated voltage	80 V
Rated speed	2500 rpm
Rated torque	1.15 Nm
Armature resistance	1.75Ω
Electrical time constant	1.5 ms
Voltage constant	28.6 V/kmin^{-1}
Nominal inertia	$5.8 \cdot 10^{-4} \text{ kg m}^2$
Viscous-friction coefficient	0.00055 Nm

The best six parameters for the CSoft-PID controller are searched in the range $[0, 20]$ by the hGASO-PS using the same procedure articulated in Section 5.3. In the algorithm, the maximum iteration number and the population size were set to 75 and 30, respectively. The final controller parameters found at the minimum value of ITAE are $K_P = 0.0116$, $K_I = 19.5627$, $K_D = 2.3752$, $N = 0.0275$, $G_1 = 1.3807$, and $G_2 = 17.0410$. The convergence profile of the algorithm is displayed in Figure 16, from which it is obvious that the best ITAE value is minimized from its initial value of 51.92 down to 47.21 through the successful

steps of the hGASO-PS algorithm. By inserting the controller parameters into the DSP, two sets of experiments are performed: (i) speed regulation and (ii) torque disturbance rejection. In the former test, speed regulation was tested, when the reference speed step amplitude was $n^* = 2500$ rpm, and the load torque was about half the rated one. The latter test aims to explore the controller’s capacity for rejection of step load disturbances. To realize this, the motor previously rotating at 2000 rpm was loaded around its rated value at $t = 1.5$ s, and later the load was removed at $t = 2.5$ s. The respective responses simulated using the CSoft-PID controller are shown in Figure 17. It is evident from this Figure that the CSoft-PID controller preserves a satisfactory speed regulation and remarkable robustness to abrupt load changes. Note that the maximum motor current was limited to ± 5 A to protect the system from excessive current.

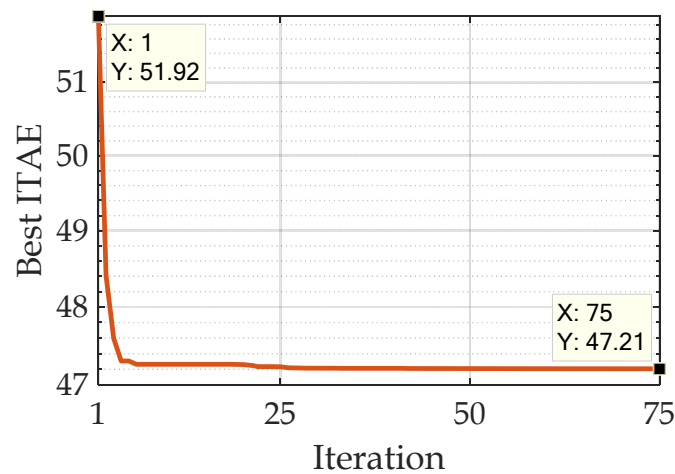


Figure 16. Convergence of the hGASO-PS algorithm for the real-time speed regulation problem of the PMDC motor.

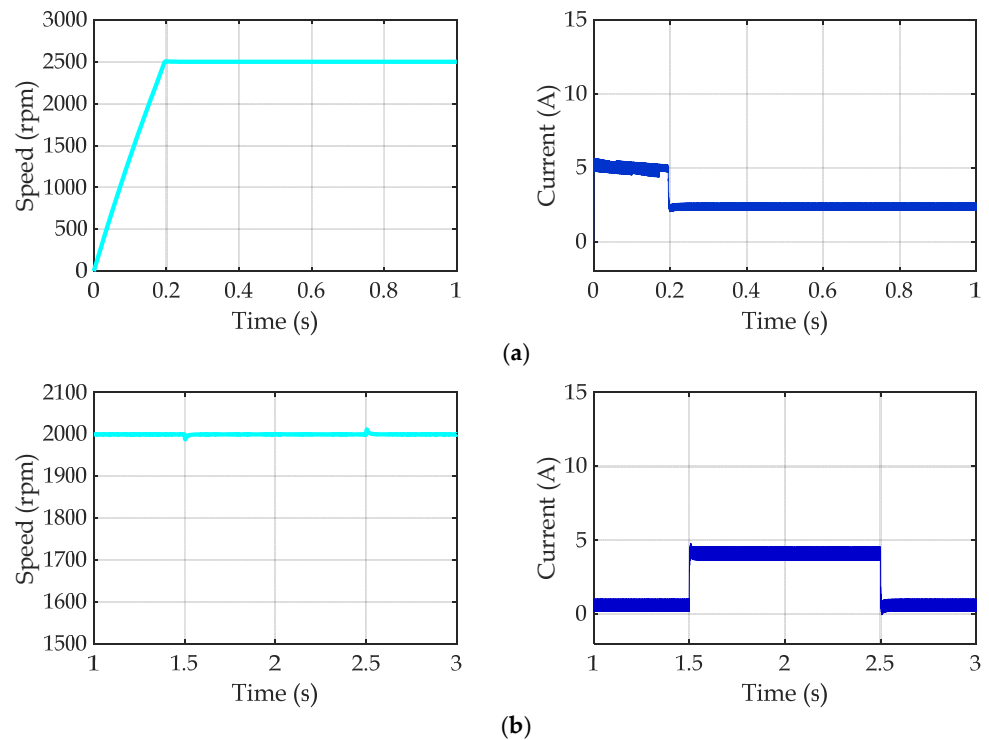


Figure 17. Simulated results under (a) a step speed command under half the rated torque, and (b) abrupt load changes.

The experimental responses complementing the above simulation analysis are provided in Figure 18. Critical observation of Figure 18 points out that the experimental responses are in very good agreement with the simulated responses in Figure 17. Like in Figure 17a, the motor accelerates quickly, and its speed settles to the reference one within 0.2 s without any sustained oscillations in Figure 18a. Likewise, the disturbance rejection profile seen in Figure 17b is very similar to what we experience in Figure 18b. Overall, by carrying out the experimental work, the proposed control scheme was validated practically. Within this context, the paper has fulfilled its goal.

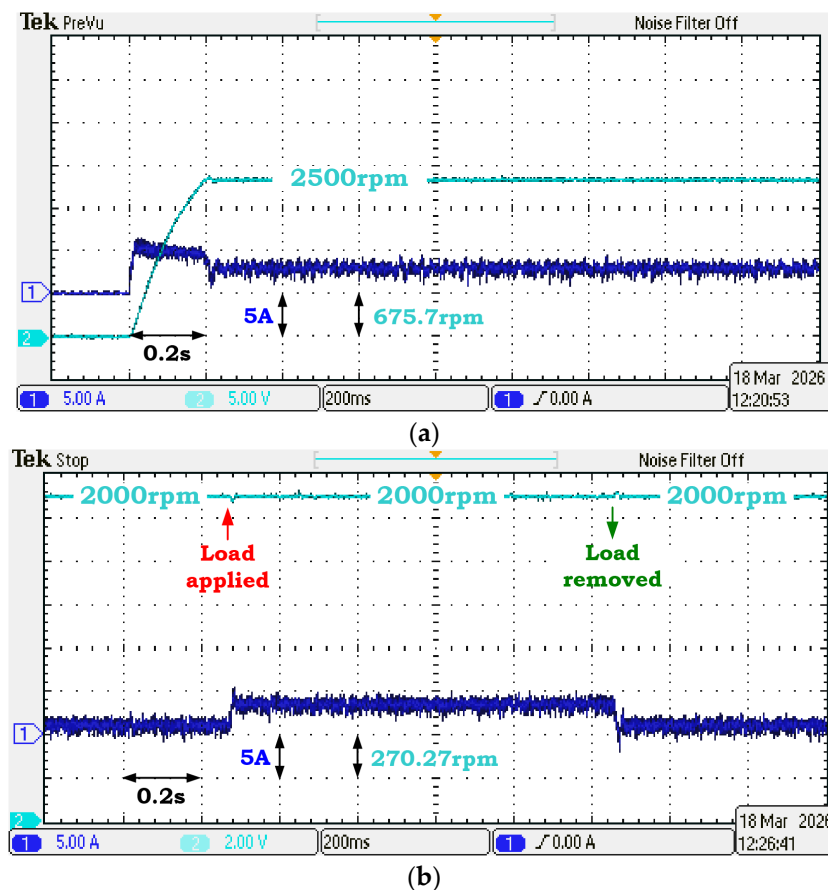


Figure 18. Experimental results under (a) a step speed command under half the rated torque, and (b) abrupt load changes.

7. Conclusions

In this study, a cascaded softsign function-based PID controller was proposed and implemented for effective pressure regulation in nonlinear shell-and-tube steam condenser systems. The proposed control structure introduces a nonlinear transformation layer into the traditional PID framework by exploiting the smooth and bounded characteristics of the softsign function. Through this mechanism, improved adaptability of the control action is achieved, enabling fine regulation around the setpoint while preventing excessive control activity during large error transients. To obtain suitable controller parameters, a hybrid optimization algorithm termed hGASO-PS was developed. By combining the adaptive global search capability of the gbest-guided atom search optimization algorithm with the local refinement ability of the pattern search method, the proposed optimizer effectively balances exploration and exploitation during the parameter tuning process. The resulting hybrid framework enables reliable identification of high-quality controller parameters within a reasonable computational effort. Extensive simulation studies were conducted to

evaluate the effectiveness of the proposed control strategy. The obtained results demonstrated clear improvements in both statistical optimization performance and closed-loop dynamic behavior. Among the five competing metaheuristic algorithms considered in the study, hGASO-PS achieved the most favorable statistical performance, with a minimum ITAE value of 2.1608, an average value of 2.2746, and a standard deviation of only 0.0934. In terms of transient characteristics, the proposed method produced the fastest settling time (12.51 s) and the lowest overshoot (1.98%), outperforming several recently reported PI, FOPID, and cascaded PI-PDN controllers available in the literature. These results indicate that the proposed controller–optimizer framework provides promising potential for nonlinear pressure regulation problems.

It should also be noted that the pressure dynamics considered in this study were represented using a simplified nonlinear model derived under ideal gas assumptions. Nevertheless, the proposed CSoft-PID structure is not inherently limited to this specific formulation. Owing to its input–output nature and cascaded nonlinear error-shaping mechanism, the controller can, in principle, be extended to more complex process models incorporating additional thermodynamic effects, nonlinear couplings, actuator limitations, or model uncertainties. However, such extensions may introduce additional challenges, including more intricate closed-loop dynamics, increased complexity in controller tuning, and the need for broader robustness validation under varying operating conditions. Consequently, the investigation of more detailed condenser models represents an important direction for future research. In addition, the present study has primarily focused on nominal closed-loop performance and optimization effectiveness under a common benchmark scenario. Dedicated disturbance rejection tests, measurement-noise sensitivity analyses, and detailed computational cost evaluations were therefore not included within the current scope of the manuscript. Although these aspects fall outside the focus of the present work, they remain important considerations for comprehensive practical validation and should be examined in future investigations to further assess the real-world applicability of the proposed hGASO-PS-based CSoft-PID framework.

Finally, several promising directions may be considered for future work. These include extending the softsign-based control concept to alternative controller structures such as fractional-order or model-predictive controllers, integrating the proposed approach with hardware-in-the-loop platforms for real-time validation, and applying the hGASO-PS optimization framework to other nonlinear processes, including thermal power plant systems, fuel cell applications, or multi-input–multi-output processes. Furthermore, the development of adaptive or self-tuning variants of the CSoft-PID controller under varying operating conditions may provide additional improvements in practical industrial applications.

Author Contributions: D.I. and S.E.: Conceptualization, methodology, software, visualization, investigation, and writing—original draft preparation; E.Ç., B.K. and E.A.: Validation, and writing—review and editing. All authors have read and agreed to the published version of the manuscript.

Funding: This research received no external funding.

Data Availability Statement: All related data are available within the manuscript.

Conflicts of Interest: The authors declare no conflicts of interest.

References

1. Marzouk, S.A.; Abou Al-Sood, M.M.; El-Said, E.M.S.; Younes, M.M.; El-Fakharany, M.K. A Comprehensive Review of Methods of Heat Transfer Enhancement in Shell and Tube Heat Exchangers. *J. Therm. Anal. Calorim.* **2023**, *148*, 7539–7578. [[CrossRef](#)]
2. Nithya, S.; Gour, A.S.; Sivakumaran, N.; Radhakrishnan, T.K.; Anantharaman, N. Predictive Controller Design for a Shell and Tube Heat Exchanger. In *Proceedings of the 2007 International Conference on Intelligent and Advanced Systems*; IEEE: Piscataway, NJ, USA, 2007; pp. 1075–1080.

3. Pandey, M.; Ramkumar, K.; Alagesan, V. Design of Fuzzy Logic Controller for a Cross Flow Shell and Tube Heat-Exchanger. In Proceedings of the IEEE-International Conference on Advances in Engineering, Science and Management (ICAESM-2012), Nagapattinam, India, 30–31 March 2012; pp. 150–154.
4. Ahn, J.-K.; So, G.-B.; Lee, J.-Y.; Lee, Y.-H.; So, M.-O.; Jin, G.-G. PID Control of a Shell and Tube Heat Exchanger System Incorporating Feedforward Control and Anti-Windup Techniques. *J. Inst. Control Robot. Syst.* **2014**, *20*, 543–550. [[CrossRef](#)]
5. Wang, J.-S.; Li, S.-X. PID Controller of Steam Condenser Based on Particle Swarm Optimization Algorithm. *J. Comput. Theor. Nanosci.* **2017**, *14*, 3698–3701. [[CrossRef](#)]
6. Somasundar Reddy, C.; Balaji, K. A Genetic Algorithm (GA)-PID Controller for Temperature Control in Shell and Tube Heat Exchanger. *IOP Conf. Ser. Mater. Sci. Eng.* **2020**, *925*, 012020. [[CrossRef](#)]
7. Al-Dhaifallah, M. Fuzzy Fractional-Order PID Control for Heat Exchanger. *Alex. Eng. J.* **2023**, *63*, 11–16. [[CrossRef](#)]
8. Schiavo, M.; Beschi, M.; Satué, M.G.; Arahal, M.R.; Visioli, A. PIDA Control of Heat Exchangers. In *Proceedings of the 2024 IEEE 29th International Conference on Emerging Technologies and Factory Automation (ETFA)*; IEEE: Piscataway, NJ, USA, 2024; pp. 1–8.
9. Jabari, M.; Ekinici, S.; Izci, D.; Bajaj, M.; Blazek, V.; Prokop, L. Efficient Pressure Regulation in Nonlinear Shell-and-Tube Steam Condensers via a Novel TDn(1 + PIDn) Controller and DCSA Algorithm. *Sci. Rep.* **2025**, *15*, 2090. [[CrossRef](#)] [[PubMed](#)]
10. Bennett, S. Development of the PID Controller. *IEEE Control Syst.* **1993**, *13*, 58–62. [[CrossRef](#)]
11. Francis, B.A. (Ed.) *A Course in H_∞ Control Theory*; Springer: Berlin/Heidelberg, Germany, 1987; Volume 88.
12. Utkin, V.I. Sliding Mode Control Design Principles and Applications to Electric Drives. *IEEE Trans. Ind. Electron.* **1993**, *40*, 23–36. [[CrossRef](#)]
13. Shah, P.; Agashe, S. Review of Fractional PID Controller. *Mechatronics* **2016**, *38*, 29–41. [[CrossRef](#)]
14. Sharma, R.; Gaur, P.; Mittal, A.P. Performance Analysis of Two-Degree of Freedom Fractional Order PID Controllers for Robotic Manipulator with Payload. *ISA Trans.* **2015**, *58*, 279–291. [[CrossRef](#)]
15. Tang, K.S.; Man, K.F.; Chen, G.; Kwong, S. An Optimal Fuzzy PID Controller. *IEEE Trans. Ind. Electron.* **2001**, *48*, 757–765. [[CrossRef](#)]
16. Al-Dhaifallah, M.; Kanagaraj, N.; Nisar, K.S. Fuzzy Fractional-Order PID Controller for Fractional Model of Pneumatic Pressure System. *Math. Probl. Eng.* **2018**, *2018*, 5478781. [[CrossRef](#)]
17. Belkadi, A.; Oulhadj, H.; Touati, Y.; Khan, S.A.; Daachi, B. On the Robust PID Adaptive Controller for Exoskeletons: A Particle Swarm Optimization Based Approach. *Appl. Soft Comput.* **2017**, *60*, 87–100. [[CrossRef](#)]
18. Suid, M.H.; Ahmad, M.A. Optimal Tuning of Sigmoid PID Controller Using Nonlinear Sine Cosine Algorithm for the Automatic Voltage Regulator System. *ISA Trans.* **2022**, *128*, 265–286. [[CrossRef](#)]
19. Ahmad, M.A.; Ismail, R.M.T.R. A Data-Driven Sigmoid-Based PI Controller for Buck-Converter Powered DC Motor. In *Proceedings of the 2017 IEEE Symposium on Computer Applications & Industrial Electronics (ISCAIE)*; IEEE: Piscataway, NJ, USA, 2017; pp. 81–86.
20. Çelik, E. Exponential PID Controller for Effective Load Frequency Regulation of Electric Power Systems. *ISA Trans.* **2024**, *153*, 364–383. [[CrossRef](#)] [[PubMed](#)]
21. Zamfirache, I.A.; Precup, R.-E.; Roman, R.-C.; Petriu, E.M. Policy Iteration Reinforcement Learning-Based Control Using a Grey Wolf Optimizer Algorithm. *Inf. Sci.* **2022**, *585*, 162–175. [[CrossRef](#)]
22. Alharbi, M.; Ragab, M.; AboRas, K.M.; Kotb, H.; Dashtdar, M.; Shouran, M.; Elgamli, E. Innovative AVR-LFC Design for a Multi-Area Power System Using Hybrid Fractional-Order PI and PID2 Controllers Based on Dandelion Optimizer. *Mathematics* **2023**, *11*, 1387. [[CrossRef](#)]
23. Behera, A.; Panigrahi, T.K.; Ray, P.K.; Sahoo, A.K. A Novel Cascaded PID Controller for Automatic Generation Control Analysis with Renewable Sources. *IEEE/CAA J. Autom. Sin.* **2019**, *6*, 1438–1451. [[CrossRef](#)]
24. Saha, A.; Dash, P.; Bhaskar, M.S.; Almakhlles, D.; Elmorshedy, M.F. Evaluation of Renewable and Energy Storage System-Based Interlinked Power System with Artificial Rabbit Optimized PI(FOPD) Cascaded Controller. *Ain Shams Eng. J.* **2024**, *15*, 102389. [[CrossRef](#)]
25. Alhosaini, W.; Aly, M.; Ahmed, E.M.; Shawky, A. Optimized Grid-Connected Three-Phase Photovoltaic Inverter System Using Cascaded FOPIT-FOPI Fractional Controller. *Energy Rep.* **2025**, *13*, 3324–3339. [[CrossRef](#)]
26. Basil, N.; Mohammed, A.F.; Sabbar, B.M.; Marhoon, H.M.; Dessalegn, A.A.; Alsharaf, M.; Ali, E.; Ghoneim, S.S.M. Performance Analysis of Hybrid Optimization Approach for UAV Path Planning Control Using FOPID-TID Controller and HAOAROA Algorithm. *Sci. Rep.* **2025**, *15*, 4840. [[CrossRef](#)]
27. Wu, Z.; Zhao, J.; Zhang, J. Cascade PID Control of Buck-Boost-Type DC/DC Power Converters. In *Proceedings of the 2006 6th World Congress on Intelligent Control and Automation*; IEEE: Piscataway, NJ, USA, 2006; pp. 8467–8471.
28. Pham, L.T.; Oksum, E.; Van Le, D.; Ferreira, F.J.F.; Le, S.T. Edge Detection of Potential Field Sources Using the Softsign Function. *Geocarto Int.* **2022**, *37*, 4255–4268. [[CrossRef](#)]
29. Jadhav, H.T.; Roy, R. Gbest Guided Artificial Bee Colony Algorithm for Environmental/Economic Dispatch Considering Wind Power. *Expert Syst. Appl.* **2013**, *40*, 6385–6399. [[CrossRef](#)]

30. El-Shorbagy, M.A.; Bouaouda, A.; Abualigah, L.; Hashim, F.A. Atom Search Optimization: A Comprehensive Review of Its Variants, Applications, and Future Directions. *PeerJ Comput. Sci.* **2025**, *11*, e2722. [[CrossRef](#)]
31. Sahu, R.K.; Panda, S.; Padhan, S. A Hybrid Firefly Algorithm and Pattern Search Technique for Automatic Generation Control of Multi Area Power Systems. *Int. J. Electr. Power Energy Syst.* **2015**, *64*, 9–23. [[CrossRef](#)]
32. Alzakari, S.A.; Izci, D.; Ekinci, S.; Alhussan, A.A.; Hashim, F.A. Nonlinear FOPID Controller Design for Pressure Regulation of Steam Condenser via Improved Metaheuristic Algorithm. *PLoS ONE* **2024**, *19*, e0309211. [[CrossRef](#)] [[PubMed](#)]
33. Li, S.-X.; Wang, J.-S. Dynamic Modeling of Steam Condenser and Design of PI Controller Based on Grey Wolf Optimizer. *Math. Probl. Eng.* **2015**, *2015*, 120975. [[CrossRef](#)]
34. Baihan, A.; Ghith, E.; Garg, H.; Mirjalili, S.; Izci, D.; Rashdan, M.; Salman, M.; Saleem, K. A Hybrid Meta-Heuristic Algorithm for Optimum Micro-Robotic Position Control with PID Controller. *Int. J. Comput. Intell. Syst.* **2025**, *18*, 86. [[CrossRef](#)]
35. Kumar, R.; Sikander, A. A New Order Abatement Method Based on Atom Search Optimization. *Int. J. Dyn. Control* **2023**, *11*, 1704–1717. [[CrossRef](#)]
36. Zhao, W.; Shi, T.; Wang, L.; Cao, Q.; Zhang, H. An Adaptive Hybrid Atom Search Optimization with Particle Swarm Optimization and Its Application to Optimal No-Load PID Design of Hydro-Turbine Governor. *J. Comput. Des. Eng.* **2021**, *8*, 1204–1233. [[CrossRef](#)]
37. Asna, M.; Shareef, H.; Muhammad, M.A.; Ismail, L.; Prasanthi, A. Multi-objective Quantum Atom Search Optimization Algorithm for Electric Vehicle Charging Station Planning. *Int. J. Energy Res.* **2022**, *46*, 17308–17331. [[CrossRef](#)]
38. Zhao, W.; Wang, L.; Zhang, Z. Atom Search Optimization and Its Application to Solve a Hydrogeologic Parameter Estimation Problem. *Knowl.-Based Syst.* **2019**, *163*, 283–304. [[CrossRef](#)]
39. Zhao, W.; Wang, L.; Zhang, Z. A Novel Atom Search Optimization for Dispersion Coefficient Estimation in Groundwater. *Future Gener. Comput. Syst.* **2019**, *91*, 601–610. [[CrossRef](#)]
40. Too, J.; Abdullah, A.R. Chaotic Atom Search Optimization for Feature Selection. *Arab. J. Sci. Eng.* **2020**, *45*, 6063–6079. [[CrossRef](#)]
41. Mohapatra, S.K.; Patnaik, S. ESA-ASO: An Enhanced Search Ability Based Atom Search Optimization Algorithm for Epileptic Seizure Detection. *Meas. Sens.* **2022**, *24*, 100519. [[CrossRef](#)]
42. Moslemzadeh, M.; Farzin, S.; Karami, H.; Ahmadianfar, I. Introducing Improved Atom Search Optimization (IASO) Algorithm: Application to Optimal Operation of Multi-Reservoir Systems. *Phys. Chem. Earth Parts A/B/C* **2023**, *131*, 103415. [[CrossRef](#)]
43. Jacob, N.; Viswanatham, V.M. Sentiment Analysis Using Improved Atom Search Optimizer with a Simulated Annealing and ReLU Based Gated Recurrent Unit. *IEEE Access* **2024**, *12*, 38944–38956. [[CrossRef](#)]
44. Mugemanyi, S.; Qu, Z.; Rugema, F.X.; Dong, Y.; Wang, L.; Mutuyimana, F.P.; Mutabazi, E.; Habumuremyi, P.; Mutabazi, R.C.; Muhirwa, A.; et al. Atom Search Optimization: A Systematic Review of Current Variants and Applications. *Knowl. Inf. Syst.* **2025**, *67*, 4813–4914. [[CrossRef](#)]
45. Reddy, C.R.; Goud, B.S.; Aymen, F.; Rao, G.S.; Bortoni, E.C. Power Quality Improvement in HRES Grid Connected System with FOPID Based Atom Search Optimization Technique. *Energies* **2021**, *14*, 5812. [[CrossRef](#)]
46. Sun, P.; Zhang, Y.; Liu, J.; Bi, J. An Improved Atom Search Optimization with Cellular Automata, a Lévy Flight and an Adaptive Weight Strategy. *IEEE Access* **2020**, *8*, 49137–49159. [[CrossRef](#)]
47. Agwa, A.M.; El-Fergany, A.A.; Sarhan, G.M. Steady-State Modeling of Fuel Cells Based on Atom Search Optimizer. *Energies* **2019**, *12*, 1884. [[CrossRef](#)]
48. Jadhav, P.P.; Joshi, S.D. Atom Search Sunflower Optimization for Trust-based Routing in Internet of Things. *Int. J. Numer. Model. Electron. Netw. Devices Fields* **2021**, *34*, e2845. [[CrossRef](#)]
49. Abualigah, L.; Izci, D.; Jabari, M.; Ekinci, S.; Saleem, K.; Migdady, H.; Smerat, A. Adaptive Gbest-Guided Atom Search Optimization for Designing Stable Digital IIR Filters. *Circuits Syst. Signal Process.* **2025**, *44*, 4059–4081. [[CrossRef](#)]
50. Huang, H.; Feng, X.; Heidari, A.A.; Xu, Y.; Wang, M.; Liang, G.; Chen, H.; Cai, X. Rationalized Sine Cosine Optimization with Efficient Searching Patterns. *IEEE Access* **2020**, *8*, 61471–61490. [[CrossRef](#)]
51. Khadanga, R.K.; Kumar, A. Hybrid Adaptive ‘Gbest’-guided Gravitational Search and Pattern Search Algorithm for Automatic Generation Control of Multi-area Power System. *IET Gener. Transm. Distrib.* **2017**, *11*, 3257–3267. [[CrossRef](#)]
52. Otieno, S.O.; Wambua, J.M.; Mwema, F.M.; Mharakurwa, E.T.; Jen, T.-C.; Akinlabi, E.T. A Predictive Modelling Strategy for Warpage and Shrinkage Defects in Plastic Injection Molding Using Fuzzy Logic and Pattern Search Optimization. *J. Intell. Manuf.* **2025**, *36*, 1835–1859. [[CrossRef](#)]
53. Yonezawa, A.; Yonezawa, H.; Yahagi, S.; Kajiwara, I.; Kijimoto, S. Fractional-order Controller Tuning via Minimization of Integral of Time-weighted Absolute Error without Multiple Closed-loop Tests. *Asian J. Control* **2026**, *28*, 20–33. [[CrossRef](#)]
54. Sowmya, R.; Premkumar, M.; Jangir, P. Newton-Raphson-Based Optimizer: A New Population-Based Metaheuristic Algorithm for Continuous Optimization Problems. *Eng. Appl. Artif. Intell.* **2024**, *128*, 107532. [[CrossRef](#)]
55. Hashim, F.A.; Houssein, E.H.; Hussain, K.; Mabrouk, M.S.; Al-Atabany, W. Honey Badger Algorithm: New Metaheuristic Algorithm for Solving Optimization Problems. *Math. Comput. Simul.* **2022**, *192*, 84–110. [[CrossRef](#)]
56. Mirjalili, S. SCA: A Sine Cosine Algorithm for Solving Optimization Problems. *Knowl. Based Syst.* **2016**, *96*, 120–133. [[CrossRef](#)]

57. Ekinci, S.; Turkeri, C.; Izci, D.; Abualigah, L.; Bajaj, M.; Blazek, V. Optimizing Steam Condenser Efficiency: Integrating Logarithmic Spiral Search and Greedy Selection Mechanisms in Gazelle Optimizer for PI Controller Tuning. *Results Eng.* **2024**, *24*, 103501. [[CrossRef](#)]
58. Ekinci, S.; Izci, D.; Gider, V.; Abualigah, L.; Bajaj, M.; Zaitsev, I. Optimized FOPID Controller for Steam Condenser System in Power Plants Using the Sinh-Cosh Optimizer. *Sci. Rep.* **2025**, *15*, 6876. [[CrossRef](#)] [[PubMed](#)]
59. Ekinci, S.; Turkeri, C.; Izci, D.; Abualigah, L.; Bajaj, M.; Blazek, V.; Prokop, L. A Novel Pressure Control Method for Nonlinear Shell-and-Tube Steam Condenser System via Electric Eel Foraging Optimizer. *Sci. Rep.* **2025**, *15*, 7550. [[CrossRef](#)]

Disclaimer/Publisher's Note: The statements, opinions and data contained in all publications are solely those of the individual author(s) and contributor(s) and not of MDPI and/or the editor(s). MDPI and/or the editor(s) disclaim responsibility for any injury to people or property resulting from any ideas, methods, instructions or products referred to in the content.